RF-SPUTTERING OF DOPED ZINC OXIDES THIN FILMS, THE EFFECT OF LOW SUBSTRATE HEATING DEPOSITION

A THESIS SUBMITTED TO

THE GRADUATE SCHOOL OF ENGINEERING AND SCIENCE

OF BILKENT UNIVERSITY

IN PARTIAL FULFILLMENT OF THE REQUIREMENTS

FOR THE DEGREE OF

MASTER OF SCIENCE

IN

MATERIALS SCIENCE AND NANOTECHNOLOGY

By
Amira Ahmed Abdelmoneam Mohamed Ahmed
January, 2017

RF-SPUTTERING OF DOPED ZINC OXIDES THIN FILMS, THE EFFECT OF LOW SUBSTRATE HEATING DEPOSITION

By
Amira Ahmed Abdelmoneam Mohamed Ahmed
Jan 2017

We certify that we have read this thesis and that in our opinion it is fully adequate, in scope and in quality, as a thesis for the degree of Master of Science.

_____

Aykutlu Dana (Advisor)

_____

Necmi Biyikli (Co-Advisor)

_____

Raşit Turan

_____

Talip Serkan Kasirga

Approved for the Graduate School of Engineering and Sciences:

_____

Assoc. Prof. Dr. Ezhan Karaşan
Director of the Graduate School

ABSTRACT

RF-SPUTTERING OF DOPED ZINC OXIDES THIN FILMS, THE EFFECT OF LOW SUBSTRATE HEATING DEPOSITION

Amira Ahmed Abdelmoneam Mohamed Ahmed
M.S. in Materials Science and Nanotechnology
Advisor: Assist. Prof. Dr. Aykutlu Dana
Jan, 2017

Zinc Oxide (ZnO) has been studied since 1930's as a candidate for the electronic applications, as it possesses a wide bandgap of 3.4 eV. While in the last 3 decades the technology of thin films were more interested in Doped zinc oxide (ZnO) for their promising potential for many applications including thin film transistors (TFTs), transparent conductive electrodes (TCEs), and thin-film photovoltaic solar cells. Mainly Indium doped and Gallium doped-zinc-oxide (IZO), (GZO) and (IGZO) thin films have drawn researchers' attention due to their remarkable electrical, optical properties, making them good candidate for the next generation flexible optoelectronic applications.

This thesis work studies the effect of deposition parameters on the crystallinity and optical properties of the thin films. In addition, the chemical composition, electrical and morphological properties of the thin films were studied in a comparative form between room temperature (RT)-grown thin films and those gown with substrate heating at 200 °C. First, a series of doped ZnO thin films were deposited by radio frequency RF-sputtering at (RT), as a function of pressure, plasma power, and argon (Ar) flow. Then a chosen deposition recipe was tested with substrate heating. Well-adhered, uniform, smooth and highly transparent films were observed. Although Literature has shown that IZO thin films exhibit amorphous nature at RT-deposition, in this work it was observed that IZO thin films exhibits crystalline nature at RT. Results indicated that low substrate heating has affected both of IZO and GZO more than it has to IGZO Thin films. The low heat effect was more effective on the

crystallinity and optical characteristics of these thin films more than its effect on their other characteristics, as it will be demonstrated as we go over each characteristic. Thicker films of (~1μm) were grown in order to evaluate the mechanical properties, including film hardness (H) and Young's Modulus (E).

Keywords: *RF-Sputtering, Doped-Zinc-Oxide, Indium Gallium Zinc Oxide, Thin Films, Low Substrate Heating, Electrical Properties, Mechanical Properties*

ÖZET
RF- PÜSKÜRTMELİ KATKILANMIŞ ÇİNKO OKSİT İNCE FİLMLER, DÜŞÜK ALTTAŞ ISITMALI BÜYÜTME ETKİSİ

Amira Ahmed Abdelmoneam Mohamed Ahmed
M.S. in Materials Science and Nanotechnology
Advisor: Assist. Prof. Dr. Aykutlu Dana
Jan, 2017

Çinko oksit (ZnO) 3.4 eV gibi geniş bir bant aralığına sahip olması ile beraber, 1930'lu yıllardan beri elektronik uygulamalar için kullanılmaktadır. Son otuz yıl boyunca ince film teknolojileri, ince film tranzistörler (TFTs), şeffaf iletken elektrotlar (TCEs) ve ince film fotovoltaik güneş hücreleri gibi uygulmalarda daha çok potansiyel vadetmesi sebebiyle, katkılanmış çinko oksit ile daha fazla ilgilenmektedir. Özellikle indiyum ve galyum katkılı çinko oksit (IZO), (GZO), (IGZO) ince filmler dikkate değer elektriksel ve optik özelliklerinden dolayı araştırmacıların daha çok ilgisini çekmekte ve yeni nesil esnek optoelektonik uygulamalar için iyi bir aday olarak göze çarpmaktadır.

Bu tez çalışması, ince filmlerde, kaplama parametrelerinin, optik özellikler ve kristallik üzerindeki etkisini incelemektedir. Ayrıca, ince filmlerin, kimyasal bileşimleri, elektriksel ve şekilsel özellikleri oda sıcaklığında ve 200°C alttaş sıcaklığı altında büyütülen filmlerde karşılaştırmalı olarak çalışıldı. Öncelikle, basınç, plasma gücü ve Argon (Ar) gaz akışı gibi kaplama parametreleri farklı değerlerde değiştirilerek, katkılandırılmış ZnO filmler seri olarak RF- püskürtmeli kaplama tenkiği ile kaplandı. Sonrasında seçilmiş bir kaplama reçetesi alttaş sıcaklığı değiştirilerek test edildi. İyi yapışmış, eş dağılımlı, pürüzsüz ve yüksek oranda saydam filmler gözlendi. Literatür IZO ince filmlerin oda sıcaklığında kaplandığında amorf bir yapıya sahip olduğunu sölese de, bu çalışmada oda sıcaklığında kaplanan IZO ince filmlerin kristal bir yapıya sahip olduğunu gösterdi. Sonuçlar, kaplama esnasında alttaşın düşük miktarlarda ısıtılmasının hem IZO hem de GZO ince filmlerde IGZO ince filmlere oranla daha etkili olduğunu gösterdi. Her bir karakterizasyon aşamasının ayrı ayrı bahsedilecek olmasıyla beraber, düşük

sıcaklığın, diğer karakterizasyonlara kıyasla; kristallik ve optik özelliklerde daha çok etkili olduğu gözlendi. Kalın filmler (~1 μm), film sertliği (H) ve elastikiyet katsayısını (E) içeren mekanik özelliklerin incelenmesi için büyütüldü.

Anahtar Kelimeler: *RF-Püskürtme, Katkılı-Çinko-Oksit, Indiyum Galyum Çinko Oksit, İnce Filmler, Düşük Alttaş Isıtma, Elektriksel Özellikler, Mekanik Özellikler*

بسم الله الرحمن الرحيم

"لَا يُكَلِّفُ اللَّهُ نَفْسًا إِلَّا وُسْعَهَا ۚ لَهَا مَا كَسَبَتْ وَعَلَيْهَا مَا اكْتَسَبَتْ"

(سورة البقرة , الاية 286)

"God does not impose on any soul a responsibility beyond its ability. Every soul receives whatever it gains and is liable for whatever it does"

(Al-Baqra Verse No:286)

That's how I know, that whatever obstacle I face, or whatever struggle is set upon me, I have the power to handle and manage the situation no matter what.

Acknowledgement

First, I'd like to thank the jury committee; Prof. Turan Raçit and Dr. Serkan Kasigra for their fruitful comments and guidance.

Special Thanks to my advisor Prof. Aykutlu Dana, for his support during the crisis I have faced here in UNAM, and for accepting me in his group. Also, thanks to my Co-advisor Prof. Necmi Biyikli.

Thanks to Dr. Eda Goldenberg for giving me the chance to get this thesis done through her project entitled "Development of ZnO Based Transparent Conducting Metal Oxides for Next Generation Applications on Flexible Substrates" funded by TUBITAK

Thanks to all my group mates Seda Kizir, Ali Haider and Turkan Bayrak for their help in this project and for sharing their knowledge.

Special thanks to my dear friends; Gulbahar Saat, Ahmed Oaf, Nour Almadhoun, Mohammed H. Alser and Zahraa Ghanem for their continuous support and for being there when I needed help the most, thanks for being in my life.

Thanks for my office mates, specially, Begimai and Ali Kalantari for his repetitive question "did you finish?" which kept me alert to finish as fast as I can just not to hear this question again, thanks for the motivation.

Huge Thanks to the one person in UNAM who made our life (foreigner students) in here a lot easier, Thanks to Duygu Kazancı for her sweet, kind and continuous support.

Thanks to Dr. Mehmet Yilmaz, and Dr. Peter for sharing their knowledge.

Thanks to my good friends; Talha Masood Khan and Murat Serhatlioglu for their help and support. Thanks Murat for translating the abstract into Turkish.

I’d like to express my sincere gratitude to my mentors; Dr. Mostafa El-Ashry, Dr. Osama Tobail and Dr. Sherif Abbas, I wouldn’t be here if not for your support and encouragement, May Allah always grant you success and happiness always.

Heartwarming thanks to my friends for life, I love to call it “*The Sisterhood of The Traveling Researcher*”. Although we are scattered all over the world chasing after our dreams, working our hearts out for our families and for our studies and research, we never let go of each other’s. Sadness or happiness, joy of grief, stressed or relaxed we have been always there for each other and still. Thanks to you gals, Nayyera Fouad, Mai Ibrahim, Ghada Antar, Mona Atta, Ghada Hamdi and Nahla Abdelshafi. No matter the distance, we will be always together. Nayyera, you are a life saver, we are all lucky to have you in our lives.

Thanks to Nashwa Moatez, Samah Elmahdy and Asmaa Foaud, I’ve learnt a lot from you and all of you mean a lot for me. I’m so happy that by the time I defended this thesis, Samah just got her master’s too. Maybe I’m the only one, who is always away, but you are always in my heart, May Allah blesses us with this special friendship forever and always.

Mam and Dad, this is for you, I would be nothing if not for your unconditional love and support. Sorry, for the sleepless night you endured for me, so I can achieve my goals and dreams. Sorry, for the times I missed to be with you. Sorry for every call I missed form you because of work and meetings. No enough “sorry” and definitely No enough “thanks” can be appreciative enough to what you have sacrificed for me and my sister and brother. This is for you Mam and Dad.

To Mam & Dad

To Sis & Bro

To you T & U ;)

Contents

List of Figures

List of Tables

Chapter 1

Introduction

1. Introduction

Z. R. Dai et al in one of the reviews stated that “Functional Oxides are the fundamentals of the smart devices”[1]. No wonder in that, since most of the nano-electronics technologies are depending on one or more of the functional oxides materials, this is not only because of their unique optical, electrical and chemical properties; but also the capability to tune these characteristics which is an application dependent request. Such characteristics make the functional oxides a diversified group of materials; that has its beneficence in many research aspects such as Superconductivity, semiconductor physics ferroelectricity and Piezoelectricity. Most studied materials are; SnO_2, In_2O_3, Ga_2O_3, ITO, CdO, PbO_2 and the different types of the doped ZnO including; AZO, GZO, IZO and IGZO[1,2]. Each of these functional oxide materials is specifically recognized for certain property. For example in terms of transparent conductive oxides (TCO), ZnO:F and Cd_2SnO_4 are recognized as highest transparency, while In_2O_3:Sn is recognized as the highest conductivity[3].

Functional oxide materials are fabricated and synthesized into many different structures and phases, depending on the fabrication methods and parameters. Such structures includes; nano-belts, nanowires, nano-sheets, and nano-diskettes[1,4–6]. Generally, the material studies of the functional oxides revolves around two aspects; first, the synthesis and fabrication methods and processes, second, the characterization of the fabricated or synthesized structures, to quantify their characteristics which in turns give insights about their proposed potential applications.

Taking that Thin films is the main focus of this work, it's convenient to shed some light on the thin film history. Starting at 1950's the thin films materials have undergone an extensive major studies that focused on their characteristics, investigating their ability to be integrated into the electronic applications and devices. That in turns, by 1960's, led to the first thin film transistor (TFT) proposed by Weimer, where he used CdS as a semiconductor thin film. As a result, more applications were proposed by 1970's; introducing novel thin film devices such as surface acoustic wave (SAW) devices and thin-film integrated optics. The silicon technology by that time has shown a promising results regarding (a-Si)-based (TFT) and a-Si solar cells. During the 1980's a speedy progress in the a-Si technology was observed as a result; a-Si solar cells were integrated into the electronic calculators as well as liquid crystal television[7].

In this work the focus is mainly on the doped zinc oxide thin films deposited by RF-Sputtering and the effect of the deposition parameters on their characteristics. Moreover, the effect of the low substrate heating deposition and its ability to be effective as the annealing process, which in turn will reduce the processes used.

1.1. Doped Zinc Oxide Thin Films

Fritsch in 1935 has fabricated polycrystalline Zinc oxide films, however not till 1960's were ZnO thin films were heavily studied, to investigate the their capabilities as piezoelectric material for acoustic wave devices[8]. Since then, ZnO have drawn the attention of the many researchers because of its remarkable optoelectronics characteristics that led them to be recognized as a promising candidate for many applications especially for transparent conductive electrodes that are for solar cells, light emitting diode (LED) and flat panel displays (FPDs)[9–12]. Over the other materials, ZnO thin films gets attention with its high transparency in the visible region (>85%), low cost, source availability, along with non-toxicity[13,14]. However, stoichiometric ZnO exhibits relatively high resistivity due to low carrier concentration and low carrier mobility[15,16]. Recently it is shown that IGZO-based thin film transistors (TFTs) are considered as a replacement for their conventional counterparts[17]. Thin films of Ga and In-Ga doped ZnO have been grown by a variety of deposition processes, including sol-gel[18,19], metal-organic chemical vapor deposition (MOCVD)[20], pulsed laser deposition[21,22], and dc and/or RF-magnetron sputtering[23,24]. Within all these techniques, RF-magnetron sputtering offers highly uniform and well-adhered thin films on large area substrates with high packing density even at low deposition temperatures. In general, it is known that the film structure, composition, electrical and the optical characteristics might be affected by the deposition parameters including (RF) plasma power, gas flow, working pressure, chamber geometry and substrate temperature.

1.2. Film Deposition and Fabrication

There is more than one classification for the thin films deposition techniques[25]. However, here we mention the most used classification. Thin film deposition techniques fall mainly under three categories, depending on the state of the materials deposited. The categories of such techniques are presented in the Fig. [1.1]. First one

is the Physical Vapor Deposition (PVD), where the material is ejected from a target and then transferred to the substrate through the vacuum. According to the type of target excitation that causes the ejection of the atoms, different systems are used. Under this category falls many systems, here are few of these deposition systems[25];

1- Thermal Evaporation, where the atoms are ejected by resistive heating, one of the draw backs is its limitation to low melting point metals. Also known as evaporative technique
2- Electron-beam Evaporation[26], as the name suggesting, in this system the atoms are ejected using an electron beam of high energy up to 30 KeV. It can evaporate any type of materials.
3- Molecular Beam Epitaxy (MBE)[27], it is known for its Knudsen effusion cells from which the element is slowly evaporated under a high vacuum of (10^{-11}) torr. These three techniques are also known as the evaporative methods
4- Sputtering, where the material targets are bombarding by Argon ions to eject the atoms, as this work was conducted with this system, it will be discussed in details in chapter two. Another classification for this, is the Glow-Discharge process[25,28].

Second category is the Chemical Vapor Deposition (CVD), where the materials are in gas form as it under goes a series of decompositions and reactions before reaching the substrates. Such technique includes; Plasma Enhanced Chemical Vapor Deposition (PECVD), Low Pressure Chemical Vapor Deposition (LPCVD), Metal-Organic Chemical Vapor Deposition (MOCVD) and Atomic layer Deposition (ALD). The third category is the Liquid Phase Deposition (LPD), such as Sol-gel and Spin Coating. The most frequently used one for the doped zinc oxides thin films is the PVD. Each of the previously mentioned categories has its advantages over the others[29,30].

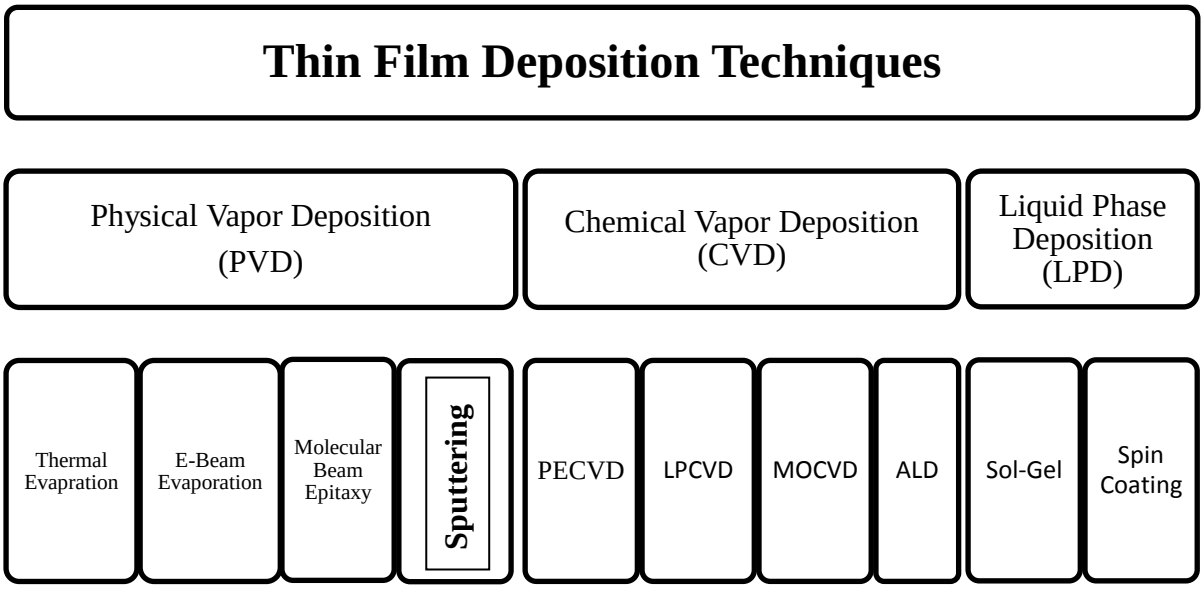

Figure 1.2-1 A diagram showing the Thin Films Deposition Techniques

1.3. Motivation

As mentioned earlier, ZnO is a candidate for the electronic applications, as it possesses a wide bandgap of 3.4 eV, however, it exhibits relatively high resistivity due to low carrier concentration and low carrier mobility, which led us to consider dopants material to tailor the thin film optical band gap as well as its conductivity. The effect of dopant materials such as aluminum (Al), indium (In) and gallium (Ga) were studied extensively through the last decade [31,32]. Among them, in particular (Ga) has shown to be less reactive and more resistant to oxidation compared to Al which makes them better dopant material [13]. Moreover, since Ga-O covalent bond length (1.92 Å) is almost similar to that of Zn-O covalent bond length (1.97 Å), Ga^{+3} can easily substitute Zn^{+2} without deteriorating the lattice[16,15,14]. On the other hand, In-Ga-ZnO doped films (IGZO) also possess excellent properties for their high carrier concentration and mobility at low cost along with high transparency and low temperature deposition processes.

Throughout the literature, two main draw backs were found, the lack of the mechanical characteristics studies for such materials and the effect of the deposition parameters on the metallic content percent in the thin films. Such draw backs were the motivation for this work. The XPS data has shown the atomic content of the metallic dopants inside the thin films as will be discussed in chapter 4 along with the mechanical characterizations of the sputtered doped zinc oxide thin films. Moreover, to investigate the effect of low substrate heating at 200 °C on the thin films characteristics and compare those to its counterpart Room Temperature (RT)-grown thin films, in terms of their characteristics and the possibility of using this low temperature for getting enhanced characteristics instead of the post-annealing process, in order to reduce the processes used.

1.4. Thesis Overview

This thesis work is composed of four chapters, where each is composed of subsections. Chapter one is the introduction where a brief intro about the functional oxide materials is presented along with the history of the thin films. Additionally, the motivation and the thesis overview are given. A detailed presentation for the experimental procedure carried in this study is demonstrated in addition to a simplified review about the main techniques and characterizations tool used in this study, is summarized in Chapter 2, where the operation principles of sputtering are pointed out along with the theory and calculations used in the interpretation of the characterization data obtained from each of the X-Ray Diffraction (XRD), Atomic Force Microscopy (AFM), X-Ray Photoelectron Spectroscopy (XPS), Ellipsometery, UV-Vis-Spectroscopy and the Nano-indentation for the mechanical characterization along with a detailed presentation for the experimental procedure carried in this study is demonstrated

The results and discussion are revealed in details in Chapter 3, where each group of the doped zinc oxide; IZO, GZO and IGZO, is expressed individually in a separate section, demonstrating the effect of the deposition parameters on the thin film characteristics. Only for GZO thin films, two groups are presented each for a different target used in the deposition. One is composed of (Ga_2O_3 / ZnO) 5/95 wt% and the other target is composed of 7/93wt%. Moreover, in a separate section the mechanical characterization is demonstrated separately. In the end, the conclusion and the future prospective are suggested in Chapter 4.

Chapter 2

Experimental Methodology

2. Experimental Methodology

The experimental part is mainly composed of two sections; the first is fabrication and film growth, where the deposition parameters and conditions are illustrated. The second is the film characterization, where the characterization tools and their data interpretation methods are explained. In this chapter a detailed description of the processes will be presented. Starting with substrate cleaning ending up with the characterization tools used. Each of IZO, GZO and IGZO, were deposited under these parameters [RF-power, (Ar) gas flow and pressure]. The main study was to develop a recipe that results in best film characteristics and then test this recipe with substrate heating at 200 ºC. Only for the GZO group, there were two targets used of different composition [5wt% and 7wt%] were used in an attempt to study the effect of the target composition on the characteristics of the deposited films especially the film composition.

2.1.Sputtering

Sputtering technique as mentioned earlier falls under many types of classifications. One of which is the PVD, as it represents the physical evaporation and deposition of the materials by using ion bombardment without any involvement of chemical reactions. Other known classification is Glow-Discharge process, where the glow-discharge is used to generate the energetic particles that strike the target causing atoms ejection. This happens in the presence of low-pressure gas that is usually argon (Ar)[33,34].

Sputtering technique itself has different systems within; such as Diode Sputtering and Magnetron sputtering. Each of these systems can be operated by both of direct current (DC) or radio frequency (RF)[28,35]. The simplest method used to be the DC-diode sputtering, where the glow discharge is guarded via dc voltage the cathode (metal target) and the anode (substrate) in the presence of Ar gas. Then the Ar^+ ions generated in the glow discharge are accelerated resulting in the sputter of atoms from the target surface and in the deposition of these sputtered atoms in form of the thin films on the substrates. However, when it comes to insulator targets DC-diode sputtering isn't the perfect choice, whereas the glow-discharge can't be maintained any longer between the metal electrodes in the presence of insulator target. The RF-diode sputtering was then introduced. The insulator target was supplied with RF-voltage to stabilize the glow-discharge during the process[33].

In magnetron sputtering[33], it's the same where it can be operated via DC or RF, where either voltage is applied between the cathode (target) and the anode (substrate) in the presence sputtering gas usually (Ar). However, the idea in magnetron sputtering is to apply a magnetic field that is parallel to the cathode (target) in order entrap the electrons and confined them in a closed loop. The magnetic field applied results in the following sequential processes:

1- Increasing the collision rate between the electrons are the sputtering gas ions.
2- Increasing the plasma density.
3- Increases the current density at the target.
4- Increases the sputtering rate

This work was carried out by using the RF-Magnetron sputtering system. As it the most common used system for doped-ZnO thin films depositions, as within all these techniques – as mentioned in Introduction chapter – the RF- magnetron sputtering offers highly uniform and well-adhered thin films on large area substrates with high packing density even at low deposition temperatures.

2.1.1. Thin Films Deposition

Using VAKSIS NanoD-4S RF magnetron sputtering system, all of doped-ZnO thin films were deposited.
Silicon (Si) (100) and glass were used as substrates for all doped-ZnO thin films depositions. Substrates were first subjected to cleaning procedure, to make sure that substrates surfaces are ready for the thin film growth. Using acetone, isopropanol and deionized water (DI), the substrates were sonicated in each, for 5 minutes to get rid of any contamination before starting the deposition.

The distance between the substrate and the target was kept constant at 14 cm. the deposition was done with constant substrate rotation to keep the uniformity of the deposited thin films. In this study, high purity argon (Ar) gas was the only gas used as sputtering gas. The sputtering chamber was vacuumed to $1x10^{-6}$ Pa for starting a proper deposition. The targets were initially sputter cleaned for 5 minutes in (Ar) atmosphere before starting the deposition in order to remove any oxide layers that might have been formed upon previous depositions as well as removing any contaminations on the surface of the targets. The targets used were; IZO target bonded on copper back support, the target purity was 99% of (In_2O_3 / ZnO) 10/90

wt%, each of the two GZO targets were bonded on copper back support, with purity 99 % of (Ga_2O_3 / ZnO) 5/95 wt% and 7/93wt% and IGZO target of purity 99% bonded on copper back support as well. Each of IZO, GZO and IGZO thin films depositions were performed in different (RF) plasma powers of 100 and 150 Watt, and different (Ar) flows of 50 and 100 sccm. The process pressure used was kept constant at 10 mtorr for IGZO thin films groups, while for IZO and GZO thin films were deposited at two different pressures of 5 and 10 mtorr. One of the recipes of each group was then subjected to substrate heating at 200 C. Table [2.1, 2.2, 2.3 and 2.4] show the recipes used for each group of the doped-ZnO thin films deposited. The deposition time was kept constant for 2 hours to determine the effect of the deposition parameters on the rate of deposition.

In order to perform the electrical characterization, metal contacts were deposited on the sides of the deposited thin films on the glass substrates. The metal contacts used were Tin (Sn) contacts. Four contacts were deposited on the edges of square shaped thin films deposited on the glass substrates.

A thicker film was grown for each of GZO and IGZO group, longer deposition time was used. Over 4 hours for GZO-5wt%, 7 hours for GZO-7wt% and 6 hours for IGZO. However, the continuous deposition for this long time interval surprisingly resulted in thick shaded films with transparency below 50%. This might be due to the high RF power used for deposition for long periods, which resulted in the formation of oxide layers over the surfaces of the target as well as the substrates. To overcome such results, a discontinuous deposition was performed for both GZO and IGZO, for intervals of 2 hours, resulted in thicker films around 900 nm. Meanwhile, the mechanical characterization was performed for the IZO thin films without the need for thicker film.

Table 2.1-1 IZO Deposition Parameters

Samples	Temp	(Ar) sccm	(RF) watt	(P) mtorr	(T) hour	Rate of growth (nm/min)	Thickness (nm)	Grain size	Trans. %
IZO-201	RT	50	100	10	2	2.55	306	27	84.3
IZO-202	RT	50	150	10	2	3.9	478	17	80.8
IZO-203	RT	100	100	10	2	2.75	330	16	82
IZO-204	RT	100	150	10	2	4.38	526	9	79.5
IZO-205	RT	100	150	5	2	2.83	340	12	80
IZO-206	200	100	100	10	2	2.93	352	20	81.4

Table 2.1-2 GZO-5wt%- Deposition Parameters

Samples	Temp	(Ar) sccm	(RF) watt	(P) mtorr	(T) hour	Rate of growth (nm/min)	Thickness (nm)	Grain size (nm)	Trans. %
GZO-201	RT	50	100	5	2	2.11	254	15	87.1
GZO-202	RT	50	150	5	2	3.3	396	21	84.3
GZO-203	RT	50	150	10	2	1.75	210	10	70
GZO-205	RT	100	150	10	2	3	356	11	54.8
GZO-206	200	100	150	10	2	3.8	460	9	74.4

Table 2.1-3 GZO-7wt%-Deposition Parameters

Samples	Temp	(Ar) sccm	(RF) watt	(P) mtorr	(T) hour	Rate of growth (nm/min)	Thickness (nm)	Grain size	Trans. %
GZO-301	RT	100	100	10	2	2.1	255	11	82.8
GZO-302	RT	100	150	10	2	2.4	290	7	88
GZO-304	200	100	100	10	2	2.2	260	10	84.8
GZO-305	200	100	150	10	2	2.6	315	7	86.7
GZO-306	200	50	100	10	2	2.2	270	9	88.8

Table 2.1-4 IGZO- Deposition Parameters

Samples	Temp	(Ar) sccm	(RF) watt	(P) mtorr	(T) hours	Rate of growth (nm/min)	Thickness (nm)	Transmission %
IGZO-201	RT	100	150	10	2	3	371	54
IGZO-202	RT	100	100	10	2	2.5	304	80
IGZO-204	RT	50	100	10	2	2.6	314	84.8
IGZO-205	200	50	100	10	2	2.58	310	86.6
IGZO-206	200	100	100	10	2	2.66	320	80.5

2.2.Thin Film Characterization Techniques

When it comes to the characterization, two questions are being asked; first what feature or characteristics do we need to study? Second, How to study this feature or characteristic? In general, Characterization of thin films is carried out to investigate their optical, electrical and mechanical properties along with their crystallinity, microstructure and chemical composition. All doped-ZnO thin films in this study were subjected to X-Ray Diffraction (XRD) to investigate their crystallinity and the estimate the grain size, Ellipsometery to determine their thicknesses and optical constants and to Carry 5000 System to determine their transmission. Whereas, selected thin films of each group of the doped-ZnO grown at RT and at 200 °C, were further subjected to each of X-ray photoelectron spectroscopy (XPS), hall measurement system, atomic force microscopy (AFM) and nano-indentation.

2.2.1. Optical and Electrical Characterization

The optical characterization was carried out by spectroscopic Ellipsometery and (UV–VIS–NIR) spectrophotometer. Spectroscopic Ellipsometery is an optical non-invasive characterization system that detects the change in polarization of the light after being reflected or transmitted from the thin films. The change of light polarization is represented by the amplitude ration (ψ) and phase difference (Δ). Since the light polarization is directly affected by both thicknesses and optical characteristics of the thin films, the reflected polarized light is detected and the data obtained is fitted through different models, giving in the exact thicknesses and optical constants of the thin films.

In this work, the thicknesses of the doped-ZnO thin films along with their optical constants were determined using angle spectroscopic Ellipsometery (V-VASE, J.A. Woollam) with rotating analyzer and xenon light source. Ellipsometery measurements were taken at multiple angles of incidence from θa=70° to 75° in 5°

steps. The optical properties were modeled using the Cauchy model and Tauc–Lorentz dispersion formula for $n(\lambda)$ and $k(\lambda)$ [32], and a three-layer model including substrate, thin film, surface roughness, and ambient. Resulting in determining the film thicknesses and their optical constants, this in turn resulted in estimating the optical band gap. The optical constants are crucial for the optical band gap calculation. As to pin out the optical band gab, first, the absorption coefficient (α) should be calculated from the famous Beer's Law:

$$\boldsymbol{\alpha = \frac{4\pi k}{\lambda}} \tag{2.1}$$

Where (α) is the absorption coefficient, (k) is the extinction coefficient and (λ) is the wavelength. By plotting $(h\nu\alpha)^2$ – Y axis- versus (hν) – X axis- the optical bandgap (E_g) is then estimated by extrapolating the linear behavior part of the plot to the X-axis of the photon energy, as shown in Fig.[3.2.6]

Thin film on glass substrate was used for the transmission characterization. This Optical transmission was measured using an ultra violet–visible–near infrared (UV–VIS–NIR) single beam spectrophotometer (Ocean Optics HR4000CG-UV-NIR) in the wavelength range of [280-900] nm relative to air.

The electrical measurements were carried out by ezHEMS Hall Effect Measurement System, where the carrier mobility, film Resistivity and carrier concentration were measured, by using the Van der pauw method. Simply metallic contacts are made on the thin films edges on the glass substrate. The thin film sample is then attached to the four contact stage, which in turns introduced into the system's chamber, where a current is then pass through the thin film in the presence of magnetic field. By knowing the thicknesses of the thin films, all of the resistivity (ρ), mobility (μ) and carrier concentration (η) are determined by the system.

2.2.2. X-ray Diffraction (XRD)

(XRD) is typically used to identify the crystalline nature of solid materials, as it identifies the degree or crystallinity, grain size, the crystal structure and orientation. Mainly an incident monochromatic X-ray is subjected to the samples, as the reflected rays have different path upon hitting different planes, a path difference is resulted. A constructive interference occurs only if this path difference is comparable to the atomic spacing, this is known as Bragg's condition or Bragg's Law:

$$\boldsymbol{2d\,Sin\theta = n\lambda} \tag{2.2}$$

Where (n) is an integer, (λ) is the incident wave length, (d) spacing and (θ) is the diffraction angle.

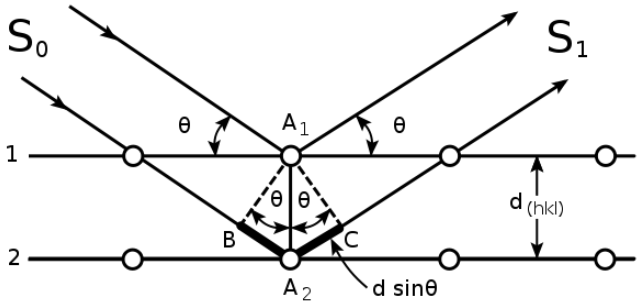

Figure 2.2-1 Bragg's diffraction

(https://commons.wikimedia.org/wiki/File:Bragg_diffraction.svg)

The doped-ZnO thin films crystallinity was determined via multi-purpose x-ray diffraction (XRD) in a PANalytical X'Pert PRO MRD diffractometer using Cu Kα (λ= 1.5406 Å) radiation, where the grain size was determined via the known scherrer's equation as shown:

$$\boldsymbol{D = \frac{0.9\,\lambda}{\beta\,cos\,\theta}} \tag{2.3}$$

Where D is the grain size, (λ=0.154 nm) is the x-ray wavelength, β is the FWHM in radians and θ is the Bragg's diffraction angle.

2.2.3. X-ray photoelectron spectroscopy (XPS)

XPS is a quantitative spectroscopic and vacuum required technique that detects the elemental composition of the samples along with their chemical and bond states. It depends on measuring the kinetic energy of the electrons emitted from the samples upon irradiating them with known X-ray wavelength. Therefore the binding energy becomes a quantitative value that can be calculated from the following conservation of energy equation:

$$\mathbf{E_b = E_p - (E_k + \phi)} \qquad (2.4)$$

Where ($\mathbf{E_b}$) is the binding energy of the electron, ($\mathbf{E_p}$) is the photon energy of the X-ray, ($\mathbf{E_k}$) is the kinetic energy of the emitted electron and ($\boldsymbol{\phi}$) is the work function which is a correction factor dependent on the instrument used. This technique detects both surface and bulk chemistry. In order to investigate the bulk, the sample undergoes etching using (Ar) ion beam.

The surface and bulk chemical compositions and bonding states of the doped-ZnO thin films RT-grown and their counterpart grown with substrate heating at 200°C , was determined by using X-ray photoelectron spectroscopy (XPS) using [Thermo Scientific K-Alpha spectrometer] with a mono-chromatized (Al Kα X-ray) source of (1486.6 eV). The samples were etched by (Ar) ion beam having an acceleration voltage of 1 kV for bulk investigation. The data of the fill scans and the elemental scan was fitted.

2.2.4. Atomic Force Microscopy and Nano-Indentation

The Surface morphology was examined for the chosen thin film using atomic force microscopes (AFM, Asylum Research MFP-3D) operating in the tapping mode using a triangular tip, where Surface roughness and grain size were estimated.

The mechanical characterization was then performed via Ambios Q-Scope AFM with nano-indentation modulus using Berkovich indenter method[36,37]. The measurement was done through one cycle of loading and unloading of a force by the nano-indenter tip, the (E) and the (H) of the deposited films were estimated from the data acquired in form of load versus displacement where the slop represents the contact stiffness (S). A schematic illustration of the indentation load is shown in Figure [2.2].

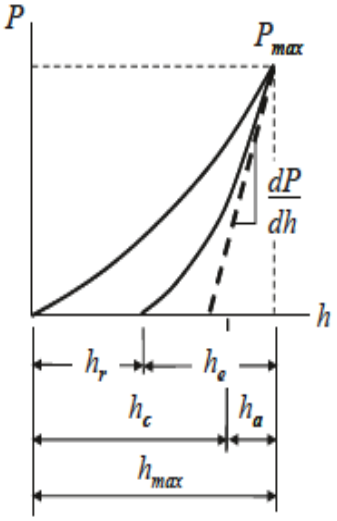

Figure 2.2-2 Schematic illustration of indentation load- displacement data [36]

The (H) was estimated from the following equation[36]:

$$H = \frac{Pmax}{A} \tag{2.5}$$

Where P_{max} is the maximum load and A is the contact area, which in case of Berkovich indenter the contact angel is 65.3º, which is represented as:

$$A = 24.5(h_e)^2 \tag{2.6}$$

Where, h_e is the plastic depth of penetration. Another formula is used to estimate the elastic modulus:

$$\frac{\mathbf{1}}{\boldsymbol{E}_e} = \frac{(\mathbf{1}-\boldsymbol{\nu}^{\mathbf{2}})}{\boldsymbol{E}} + \frac{(\mathbf{1}-\boldsymbol{\nu i}^{\mathbf{2}})}{\boldsymbol{Ei}} \tag{2.7}$$

Where (E_e) is the effective modulus, this effective modulus is the actual elastic displacement that occurs in both the thin films and the indenter, each with its own elastic modulus and Poisson's ratio; (E, ν) and (E_i, ν_i) for the sample and the indenter respectively.

Chapter 3

Results and Discussion

3. Results and Discussion

This chapter is composed of 4 sections, 3 of which are designated to a material group of doped-ZnO thin films characterization, while the fourth section is for the mechanical characterization. The structure of all the sections, is almost the same for the 3 groups [IZO, GZO and IGZO], the common structure is as follow; first, the effect of deposition parameters [RF-power, (Ar) flow and process pressure] on the crystallinity and the optical characteristics are being discussed in the beginning of each section of each material. Then a comparison is stated between the RT-grown thin films and the 200°C- grown thin films for each of; crystallinity and the optical characteristics, chemical composition, bond state and electrical properties, ending with morphological and mechanical properties.

3.1. Indium Zinc Oxide Thin Films (IZO)

The first material to be discussed in this study is the Indium doped Zinc Oxide Thin films (IZO). The IZO target that was used was bonded on copper back support, the target purity was 99% of (In_2O_3 / ZnO) 10/90 wt%. This group of thin films is composed of 6 samples, 5 of which are grown in RT while 1 sample was grown at 200°C. The structure of the result starts with the effect of RF-power at two different values of (Ar) flows and vice versa at constant process pressure of 10 mtorr, then the effect of process pressure at constant RF-power and (Ar) flow of 100 watt and 100 sccm respectively. After which a comparison is stated between thin film grown at RT and that grown at 200°C, regarding their crystallinity and the optical characteristics, chemical composition, bond state and electrical properties, and finally their morphological and mechanical properties.

3.1.1. Crystallinity and Optical properties

It's known that the XRD patterns for sputtered ZnO thin films exhibits hexagonal wurtzite structure with c-axis orientation with dominant diffraction crystal peak of (002) at 35.4° [16,15,14,38]. And so apparently the doped ZnO thin films show the same characteristics. It's worth mentioning that for the last decade the literature has shown that the IZO films grown at room temperature are amorphous[39–45], and the diffraction peaks would appear at higher growth temperatures starting at 400 °C or higher doping values of (In) [46]. However, in this study all the room temperature grown IZO thin films have shown the crystalline peak corresponding to the (002) plan, with different intensities as shown in Fig [3.1.1]. The (002) peak was the only dominant peak for all the grown IZO thin films, and no other peaks were observed.

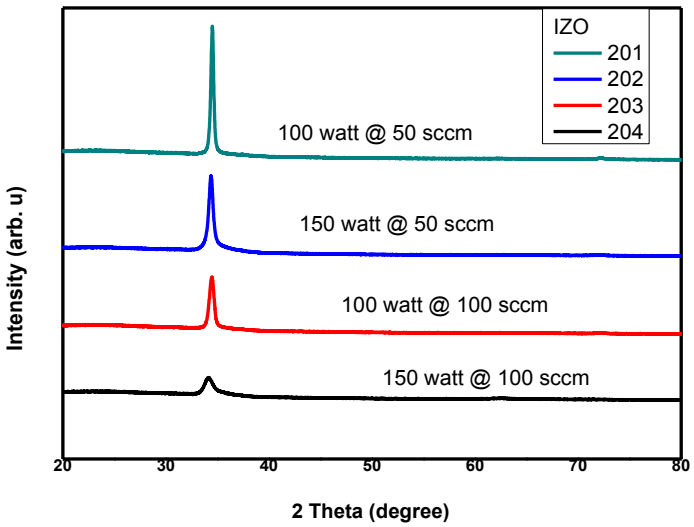

Figure 3.1-1 XRD Pattern of RT-grown thin films of IZO

All of the IZO thin films exhibit hexagonal wurtzite structure as expected. While keeping the process pressure constant at 10 mtorr, two values of RF-power were used (100 and 150 watt) once at 50 sccm of (Ar) flow and another at 100 sccm. It's noticeable that higher RF-power decreases the intensity of the diffraction peak, along which the grain size decreases as well. The same observations were obtained while monitoring (Ar) flow, where the intensity of the diffraction peak decreased as well with increasing the (Ar) flow. It's worth mentioning that there was no significant shift in the (002) peak angle, where the shift was only in order of 0.2° and 0.3° toward lower angle in case of increasing the RF- power at 50 sccm and 100 sccm (Ar) flow respectively. The calculated Grain Sizes are mentioned in Table [2.1]. This is came in contradiction with the GZO and IGZO results were the RF-power increment resulted in enhancement of the crystallinity of the thin films as it will be discussed later in this chapter in the GZO and IGZO thin film results section. In fig [3.1.2] the XRD pattern of two thin films RT-grown at different process pressure [10 and 5] mtorr.

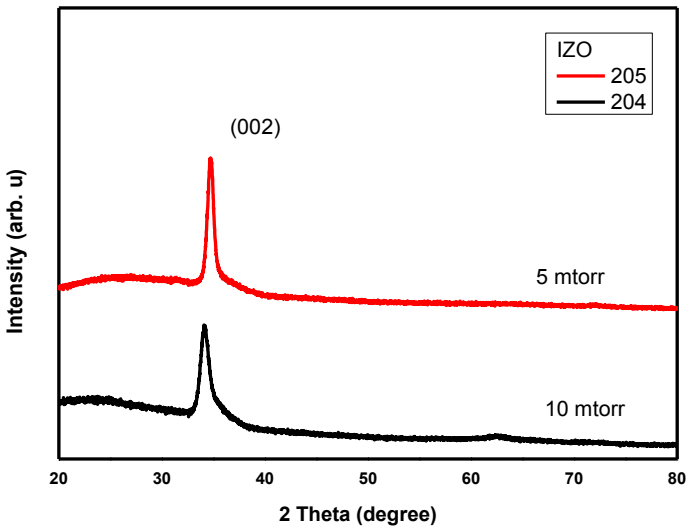

Figure 3.1-2 XRD Pattern of IZO thin films at different process pressures

Decreasing the process pressure to 5 mtorr has increased the intensity of the dominant (002) peak when compared to the 10 mtorr-grown thin films. Moreover a shift toward higher diffraction angle by 0.7° was observed in case of decreasing the process pressure to 5 mtorr. The 200° C grown thin film (IZO-206) was deposited at 100 watt for RF-power, 100 sccm (Ar) flow and 10 mtorr process pressure which are the same deposition parameters as for sample (IZO-203) except for the growth temperature. Fig [3.1.3] shows the XRD patterns of IZO thin films grown under same parameters except for the temperature. The changes observed were first the intensity of the (002) peak increased, second the grain size increased from 16 nm to 20 nm representing RT-grown thin film and the 200 C grown thin film respectively.

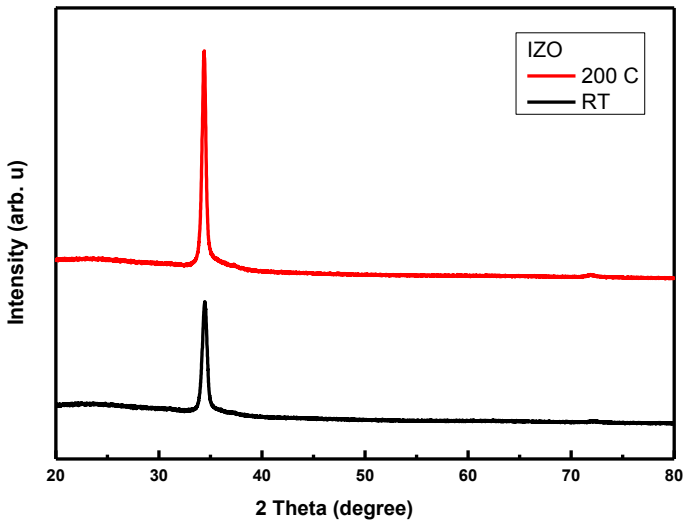

Figure 3.1-3 XRD patterns of IZO thin films grown at RT and 200 °C

For all the IZO thin films XRD patterns, no metallic peaks have been observed; neither for Zn or (In) indicating that (In) atoms is well incorporated into the thin films substituting the Zn atoms, and that the thin films are fully oxidized.

Ellipsometery measurements were taken at multiple angles of incidence from θa=70° to 75° in 5° steps. The optical properties were modeled using the Cauchy model and Tauc–Lorentz dispersion formula for $n(\lambda)$ and $k(\lambda)$, and a three-layer model including substrate, film, surface roughness, and ambient. The results defined the film thicknesses and their optical constants; this in turn resulted in estimating the optical band gap. The thicknesses of the IZO thin films are shown in Table [2.1]. The rate of deposition hasn't change much upon changing neither the process pressure nor the (Ar) gas flow, were it kept swinging from [2.5 to 2.9 nm/ min]. However, the rate of deposition has jumped to 3.9 nm/min and 4.3 nm/min upon using RF-power of 150 watt at 50 Sccm and 100 sccm (Ar) gas flow respectively, showing that the RF-power has a significant effect on the rate of growth, that might be due the increases of the ionization efficiency, which results in trapping more electron in the plasma in the vicinity of the substrate, resulting in higher deposition

rate [34]. The (E_g) hasn't change much compared to GZO, as will be discussed later, where it kept swinging between 3.3 eV to 3.38 eV over the change of deposition parameters. Apparently, tailoring the band gap of ZnO thin films using (In) doping is not quite significantly. The optical bandgaps (E_g) are represented in table [3.1.1].

Table 3.1-1 Optical Bandgap and Transmission of IZO Thin Films

IZO Thin Films	E_g (eV)	Transmission %
IZO-201	3.32	84.4%
IZO-202	3.33	80.8%
IZO-203	3.34	82%
IZO-204	3.4	79.5%
IZO-205	3.37	80.2%
IZO-206	3.38	81.4%

In fig [3.1.4] and fig. [3.1.5], the optical constants [(n) and (k)] are shown for all the IZO thin films. It can be seen that the refractive indices of all the IZO thin films are similar in the visible region except for the film grown under 200 °C, were its refractive index decreased. While in the infra-red region the refractive indices showed higher values for grown under 5 mtorr sccm, and the lower value for the thin film grown under 10 mtorr process pressure both thin films were grown under RF-power of 150 watt and 100 sccm (Ar) flow. The Extinction coefficient (k) were observed to be similar as well for all of the IZO thin films over the visible region, while it varies over the infra-red region.

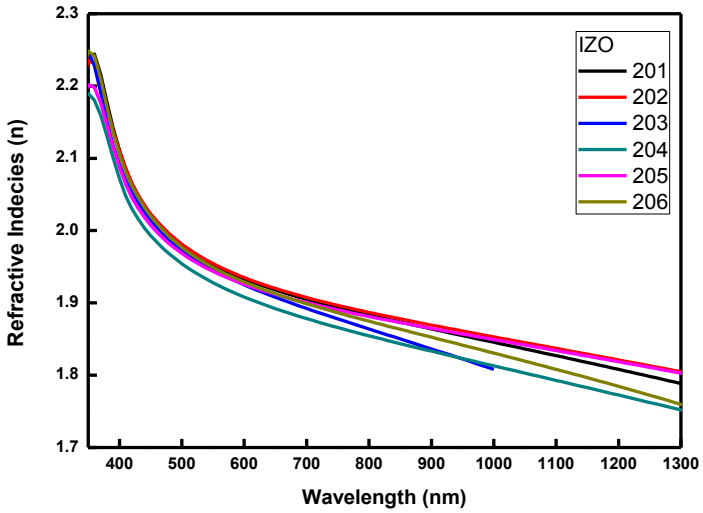

Figure 3.1-4 IZO thin films refractive indices

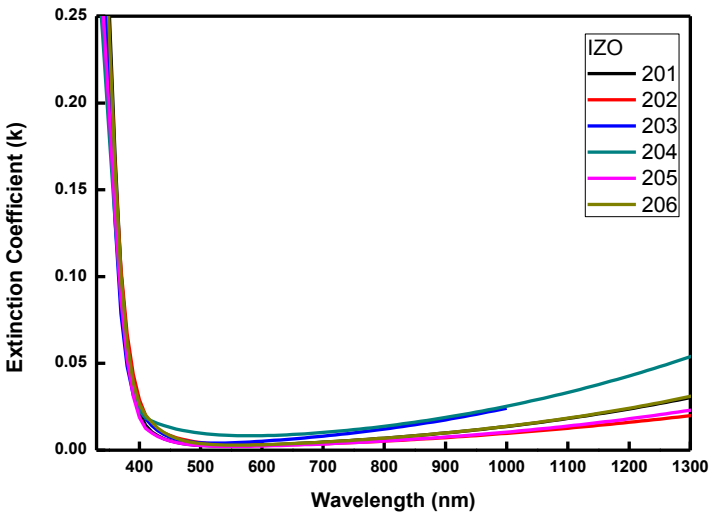

Figure 3.1-5 Extinction Coefficients (k) of IZO Thin Films

All the IZO thin films were highly transparent over the visible region recording transmission > 85%. Fig [3.1.6] represents the transmission spectra of the IZO thin films over the range of [280 – 900] nm. As seen there is only a small blue shift which agrees with the small changes over the optical band gap, extrapolated from the Ellipsometery data analysis. This blue shift according to Burestin-Moss repost, known as BM-Shift, is an indication for the increase of carrier concentration that is attributed with the increase of optical bandgap[43,47].

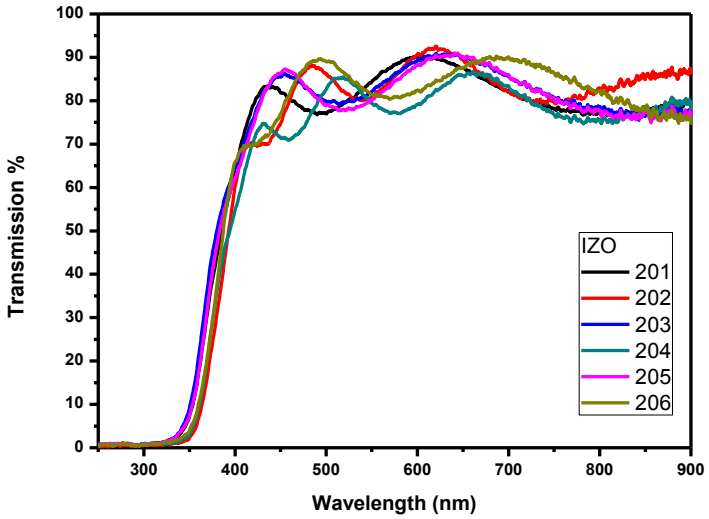

Figure 3.1-6 Transmission Spectra of IZO Thin Films

3.1.2. Chemical Composition, Bond State and Electrical properties

Generally, X-Ray Photoelectron Spectroscopy was performed for the two thin films of each group of material. These two samples were deposited under same condition except for the temperature, where one is RT-grown while the other is grown at 200 °C. The two thin films have shown the following peaks; Ar 2p, C 1s, O 1s, Zn 2p and In 3p. The presence of the Ar 2p peak was an indication for a slight contamination within the XPS-chamber.

For O 1s, the peak positions are known to be classified typically into three main binding energy regions; low binding energy (BE) centered at 530.35 ± 0.3, medium BE at 531.31 ± 0.3 and high BE at 532.25 ± 0.3, each attributed to O^{-2} ions in the lattice, O^{-2} in the oxygen deficient regions and the chemosorbed oxygen on the surface either absorbed O^2 or adsorbed H_2O respectively[10,48,49]. After fitting the data, the IZO thin films O1s peak was observed at lower (BE) and it was centered at 530.4 eV which is consistent with the O^{-2} ions within the lattice. There was no noticeable shift in the peaks for the thin film grown at 200 C. Moreover both films didn't show any metallic peaks either for Zn or In, which indicate that both are on the oxide states, which in turns agrees with the XRD findings.

Thin films deposited on glass substrates were used for the electrical characterization via ezHEMS Hall system, where a four metal contacts were made on top of the thin films. Using van der pauw, a current was applied to the thin films in the presence of magnetic field, to determine the electrical characteristics of the IZO thin films. According to C. Lee et al. annealing at high temperatures >200 has a tendency to change the resistivity significantly, because the variation in resistivity due to the microstructural change, are based on thermally activated processes[43]. He has shown that amorphous IZO thin films sputtered by RF and annealed at 200 C acquired a low resistivity of 6.2 X 10^{-4} Ω.cm [39]. In this study, thin films grown at RT possess low resistivity, were the measurement recorded 5.97 X 10^{-4} Ω.cm, and

carrier concentration of 7.59 X 10^{20} cm^{-3} along with mobility of 2.75 V.cm.s. Here the results of RT-grown thin filsm were comparable to those annealed. As shown in [table 3.1.3] all the electrical characteristics of the IZO thin films are presented.

Table 3.1-2 Transmission of IZO Thin Films

Samples	Temp	(Ar) sccm	Power watt	(P) mtorr	Grain size nm	Transmission %
IZO-201	RT	50	100	10	27	84.4
IZO-202	RT	50	150	10	18	80.8
IZO-204	RT	100	150	10	9	79.5
IZO-205	RT	100	150	10	12	80
IZO-206	200	100	100	10	20	81.4

Table 3.1-3 IZO thin films Electrical Properties

Samples	Thickness (nm)	Resistivity (σ) (Ω.cm)	Carrier Conc. (η) (cm^{-3})	Mobility (μ) ($cm^2. V^{-1}.S^{-1}$)
IZO-201	306	4.15×10^{-3}	7.49×10^{19}	2.94
IZO-202	478	6.03×10^{-3}	1.09×10^{20}	9.54
IZO-204	526	5.97×10^{-4}	7.59×10^{20}	2.75
IZO-205	340	1.12×10^{-3}	7.89×10^{20}	1
IZO-206	352	5.08×10^{-3}	5.54×10^{20}	2.22

Apparently, the higher mobility was seen in thin film grown at 150 watt RF-power, 50 sccm (Ar) flow and process pressure of 10 mtorr, presented by thin film IZO-204. As shown the mobility increased from 2.94 to 9.54 $cm^2. V^{-1}.S^{-1}$ when the RF-power increased from 100 watt to 150 watt; however it falls back to 2.75 upon increasing

the (Ar) flow up to 100 sccm as in thin film IZO-204. Moreover, the mobility deceases further when the process pressure dropped to 5 mtorr, where it possesses (1 cm^2. $V^{-1}.S^{-1}$) which is very low compared to the records in literature which is reported in the range of (~5 to 10 cm^2. $V^{-1}.S^{-1}$) [46]. We see here that the sensitivity decreased by an order of one magnitude to drop from 6.03 x 10^{-3} to 5.97 x 10^{-4} (Ω.cm). As shown, this decrease in resistivity was on the expenses of the mobility which dropped apparently from (~10 to ~ 2 m^2. $V^{-1}.S^{-1}$).

3.1.3. Morphological Structure

2D AFM images of IZO thin films of 1µm x 1µm are shown in fig [3.1.7], for both grown at RT and at 200 C. its known that amorphous IZO thin films acquire low RMS > 1 nm[41,50]. The thin films showed that they exhibit high surface roughness; this might be because the thin films exhibit poly-crystalline rather than amorphous characteristics as it was indicated from the XRD. It appears that the thin film deposited at low (Ar) flow of 50 sccm has shown RMS of 4.22 nm. And as the (Ar) flow increased up to 100 sccm, the RMS was increased up to 5.37 nm. Moreover the RMS also increased significantly upon increasing the RF-power to 150 watt, resulting in RMS of 6.96 nm. The thin film grown at 200 °C showed roughhouses of 3.88 nm, which is lower than those of the RT-grown thin films, however, thin film deposited at RT but at low process pressure of 5 mtorr instead of 10 mtorr, has shown the lowest RMS among the rest of the IZO thin films, giving RMS of 1.66. This is an indication process pressure has a major effect on the roughness of IZO thin films and that they can be tailored upon the desired application as the case of organic light emitting diodes (OLED), that requires transparent thin films of low surface roughness, which is found to be a critical aspect for the OLED life time performance[50] and in terms of flexibility[51].

a) b)

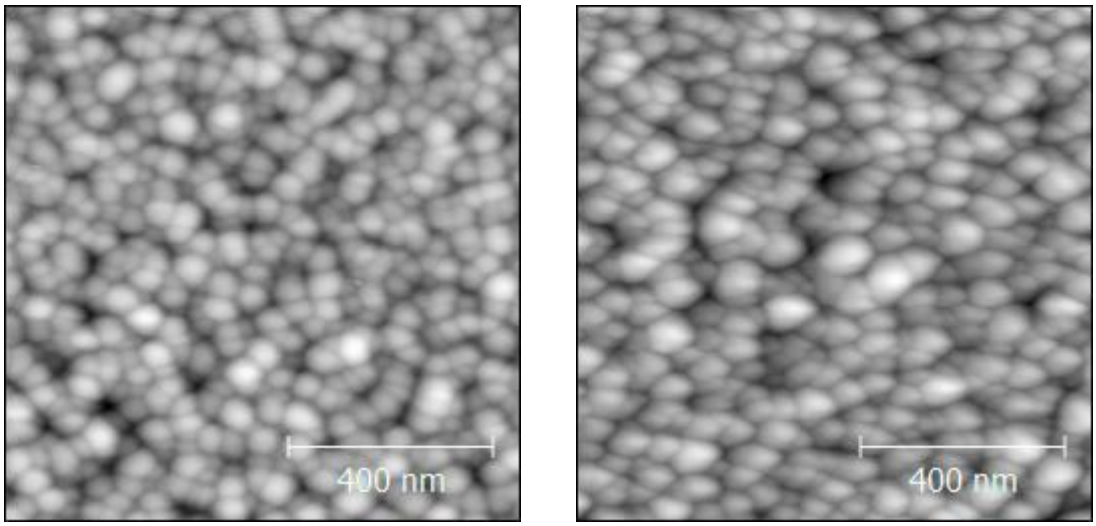

Figure 3.1-7 IZO thin film 2D AFM images, a) RT-grown, b) 200 °C

3.2. Gallium Zinc Oxide Thin Films (GZO)

The second material of this study was GZO, where two targets each bonded on copper back support, with purity 99 % of (Ga_2O_3 / ZnO) 5/95 wt% and 7/93wt%, were used for the thin films depositions. The structure of this section is the same as previous, as a starting point, the optical properties and crystallinity of the films are demonstrated followed by, the film composition and bond state, morphology and electrical properties. Each of these characteristics is discussed with respect to the parameter involved in their deposition. Since this section is for two groups of different target compositions, the thin film groups are assigned as GZO-5wt% and GZO-7wt% to differentiate between the two groups.

3.2.1. Crystallinity and Optical properties

It's known that the XRD patterns for sputtered ZnO thin films exhibits hexagonal wurtzite structure with c-axis orientation with dominant diffraction crystal peak of (002) at 35.4°[16,15,14,38]. Starting with GZO-5wt%, XRD pattern for the GZO thin films deposited at different parameters are presented in figures [3.2.1, 3.2.2 and 3.2.3] for different RF powers, different pressure and different Ar flow respectively. All of the GZO thin films exhibit hexagonal wurtzite structure as expected. However, three peaks of (100), (002), and (101) have appeared with different intensities in most of the samples indicating that the thin films of GZO-5wt% acquire polycrystalline hexagonal wurtzite structure and the variation in the diffraction lines of the three peaks indicate that the thin films acquire asymmetry crystallite [16]. (002) peak was dominant only in case of the deposited thin film at pressure of 5 motrr.

As shown in Fig [3.2.1] two main features are observed upon increasing the RF-Power, first is that the (002) peak shifted toward the left to lower diffraction angle from 34.4° to 33.2°, second is that the intensity of the (002) peak is significantly increased. This indicates that the film crystalline features have enhanced with the RF-power increment, however the shift to the lower diffraction angle is suggested to

be due to the increase in the inter-planer spacing[38]. The grain size was calculated using scherrer's equation, giving 15.5 nm for the sample deposited at 100 watt and 21.6 nm for the thin film deposited at 150 watt, which shows that as the power increase the grain size increases as well. In figure [3.2.2] where the films deposited at different pressures of 5 mtorr and 10 mtorr are shown, the features observed are that the film shifted to higher angle with increasing the pressure from 33.2° to 34.2°. Moreover, two other diffraction peaks (100) and (101) were observed, indicating that the crystallinity and epitaxiallity of the thin film is decreasing as the pressure increasing [14].

Although that the presence of these additional diffraction peak indicates less crystalline and less epitaxial thin film, the grain size was significantly decreased from 21 nm to 10 nm. The same three peaks of (100), (002) and (101) were observed for the films deposited at different (Ar) gas flow of 50 and 100 sccm. The grain size was slightly differed from the 50 sccm to 100 sccm by 1 nm, where the film deposited at 50 sccm acquired grain size of 10.2 nm while the film deposited at 100 sccm acquired grain size of 11.4 nm. It's clear that for GZO-5wt% group two contradictory observations have been shown upon increasing RF-power and increasing the pressure, where the diffraction peak (002) which was the dominant peak only in case of the high power, has shifted to the lower angle in case of the higher RF-power while for higher pressure the diffraction peak shifted to higher angle. For grain size, it was observed that it increases as the RF-Power increasing while decreases as the pressure increases.

All these observation indicate that the crystallinity in enhanced with high RF-power and low pressure. While the difference in the (Ar) used didn't have any significant effect on either the crystallinity or the grain size. For the thicker sample of 900 nm deposited for the mechanical characteristics, many other diffraction peaks have slightly appeared as shown in fig [3.2.4], indicating the loss of epitaxiallity along with the crystallinity of the films at higher thickness. This might be a result of the discontinuous time interval of deposition.

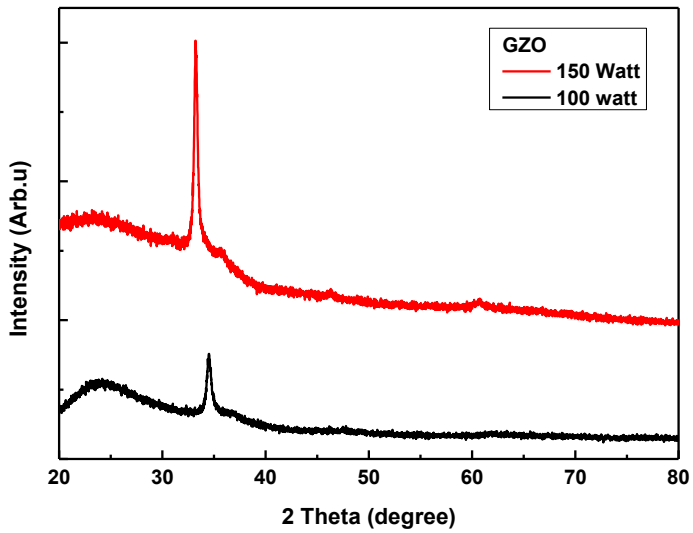

Figure 3.2-1 XRD Pattern of GZO thin films Deposited at different RF powers

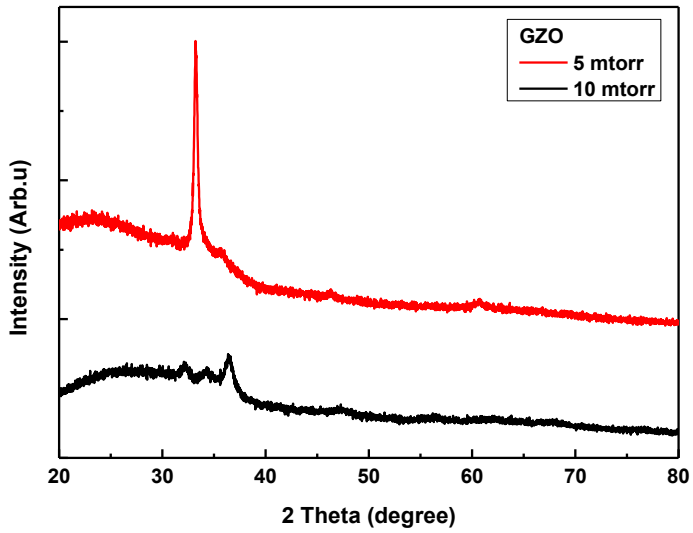

Figure 3.2-2 XRD Pattern of GZO thin films Deposited at different pressures

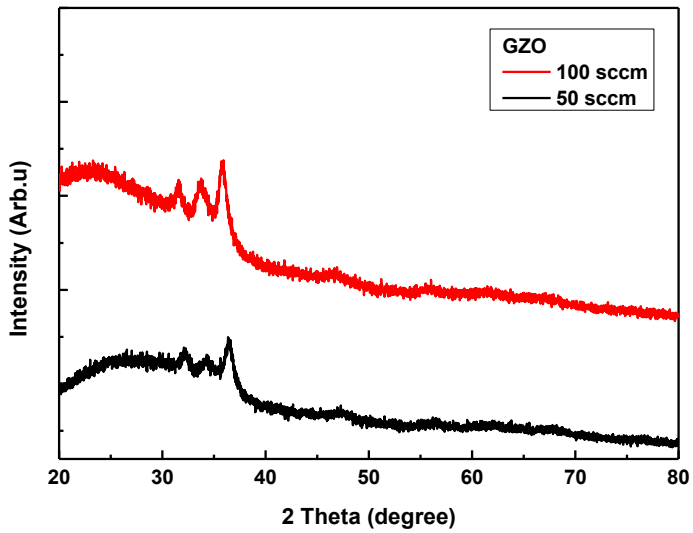

Figure 3.2-3 XRD Pattern of GZO thin films Deposited at different (Ar) flows

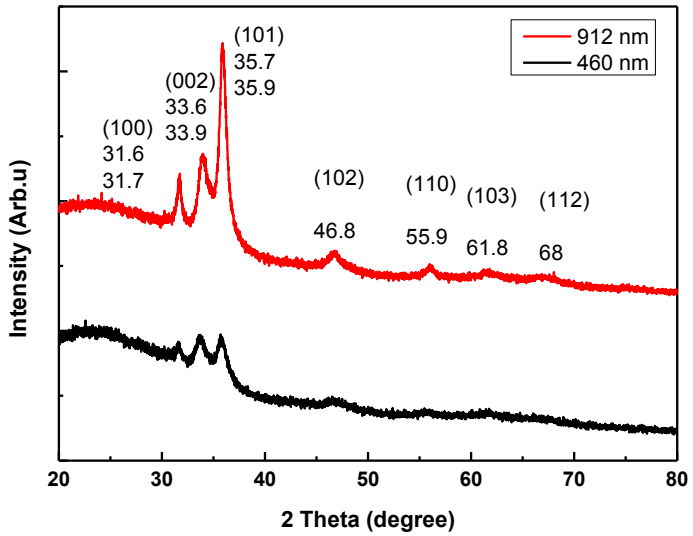

Figure 3.2-4 XRD Pattern of GZO-wt5% thin films of different thickness

Regarding the GZO-7wt% thin film group, as mentioned earlier also exhibits hexagonal wurtzite structure with c-axis orientation with dominant diffraction crystal peak of (002) with no additional diffraction peaks observed. In all GZO-7wt% thin films, one dominant peak appeared at (002) with no additional peaks, however the intensity of this peak changes upon the change in the deposition parameters. The effect of RF power is shown in fig [3.2.5] that represents the XRD pattern of GZO-7wt% thin films deposited at 100 watt and 150 watt. The intensity of the diffraction peak decreased with the higher deposition power that results in an increase in the FWHM values, which in turn decreased the grain size from 11 nm to 7 nm; moreover there was a slight shift to the left in the diffraction peak towards lower angle with the higher RF-power. Since 100 watt sample showed relatively better crystallinity, the recipe was tested directly with substrate heating at 200 °C.

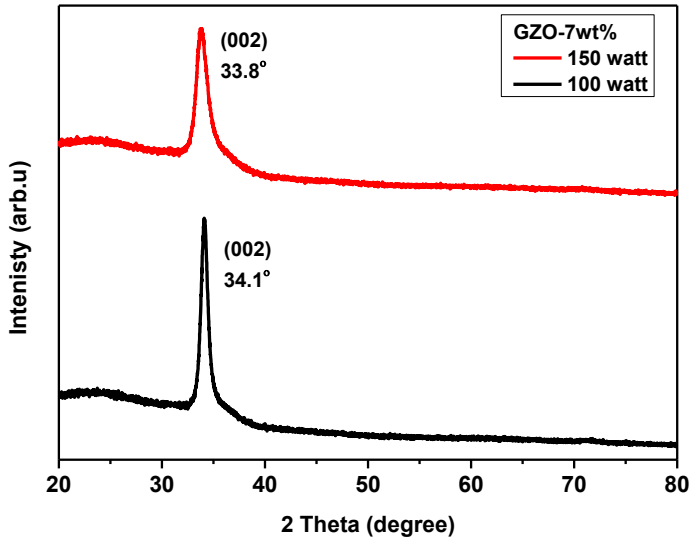

Figure 3.2-5 XRD Pattern of GZO-7wt% thin films deposited at 100 and 150 watt

All the XRD patterns of GZO thin films didn't show any metallic zinc or gallium peak indicating that Zn^{+2} was substituted with Ga^{+3} without deteriorating the lattice[16,14,38].

As mentioned in the methodology section the optical data obtained by the Ellipsometery measurements that was taken at multiple angles of incidence from θa=70° to 75° in 5° steps. The Results showed the film thicknesses and their optical constants, this in turn resulted in estimating the optical band gap. First the thicknesses were determined as shown in Table [2.2 and 2.3] for both GZO-5wt% and GZO-7wt% respectively. Apparently, the rate of deposition increased as the RF-power used increased. Upon increasing the RF-power the ionization efficiency increases as well by trapping more electron in the plasma in the vicinity of the substrate, resulting in higher deposition rate[34]. The case was the same for increasing the reactive Ar gas flow, the rate of deposition increased with Ar flow increment, because this increment provides high flux of ions.

Moreover as it appears in table [3.2] for GZO-5wt% the rate of deposition decreased significantly upon increasing the pressure which is expected, as the pressure increases the sputtered ions are subjected to more collisions before reaching the substrates leading to lower rates of depositions[34]. After film thicknesses determination, the optical constants were determined in turns, by which the optical band gap was estimated for the thin films by the plotting $(\alpha h\nu)^2$ versus $(h\nu)$, where (α) is the absorbance and $(h\nu)$ is the energy in eV. It appears that the (E_g) has increased significantly while increasing both RF-Power to 150 watt, 100 sccm (Ar) flow in case of GZO-5wt% thin film group, where it jumped from [3.3 eV to 3.5 eV and 3.75 eV] due to the increases of RF-power and (Ar) flow respectively.

The case was not the same for the GZO-7wt% as the change in (E_g) was in terms of 1 eV due to higher RF-power and only 0.5 eV due to higher (Ar) flow. Apparently, the same deposition parameters [100 sccm/ 150 watt/ 10 mtorr] have yielded the same (E_g) in both GZO-5wt% and GZO-7wt% which is 3.75 eV the highest among all the samples in both groups. Moreover, depositions parameters didn't have much

effect on tailoring (E_g) in case of GZO-7wt% as much as it affected the GZO-5wt% group.

Table 3.2-1 GZO Thin Films Optical Bandgap (Eg)

GZO-5wt%	**(E_g) (eV)**	**GZO-7wt%**	**(E_g) (eV)**
GZO-201	3.3	GZO-301	3.65
GZO-202	3.5	GZO-302	3.74
GZO-203	3.37	GZO-304	3.6
GZO-205	3.75	GZO-305	3.63
GZO-206	3.38	GZO-306	3.7

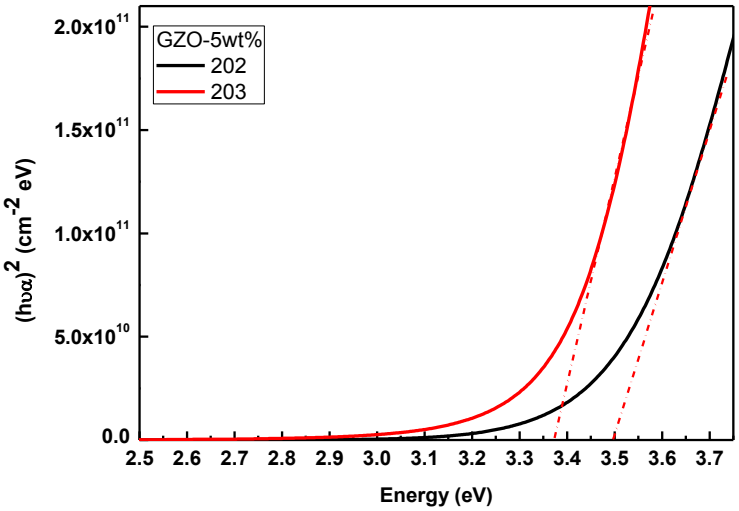

Figure 3.2-6 Plot of $(\alpha hv)^2$ versus (hv) to estimate the bandgap by extrapolation

The transmission spectra of the deposited films are shown in fig. [3.2.7]. the transmission spectra is shown over [280-900] nm. The spectra have shown to exhibit fine oscillating transmittance curves, expressing the homogeneity of the thin films and their low surface roughness[52,53]. In the visible region (400-700) the transmission were recorded to be above 75% as mentioned in Tables [2.2, 2.3] for GZO-5wt% and GZO-7wt% respectively. However, unexpectedly, film deposited at

higher RF-power and higher (Ar) flow showed low transmission around 60% which later was enhanced by using the substrate heating, that will be explained in details in section 4.4. Mainly the transmission spectrum in this study has two important regions as shown; the first one is the cut-off edge at the blue side, where there is a hilly drop at the transmission, which is here below 350 nm for all the GZO thin films, however there is a slight shift in the range of 20 nm to the right, between the films deposited at low pressure and low (Ar) flow and those deposited at higher pressure and higher (Ar) flow. This indicates the change over the optical band gap. As the shift is to the higher energy, which is attributed to the increase in the carrier concentration that fills the ZnO small density states near the conduction band minimum resulting in an increase in the bandgap energy that also indicate the transition between the valence band and the conduction band [11,16].

The second region in the transmission spectrum is the visible region (400-700), the majority of the samples have shown transparency > 80% that agrees with the literature, except for the one sample in GZO-5wt% group that has shown 60% transmission, in which the substrate heating had a drastic improvement for the transmission to jump from 60% to 75% indicating that the Ga content in the films were not oxidized at the room temperature deposition and that substrate heating helped in oxidizing the rest of Ga content on the thin film. GZO-7wt% group thin films transmissions were >85% as shown in Table 3.3 and figure [4.2.8] The changeover transmission due to different deposition parameters was in terms of 5% change.

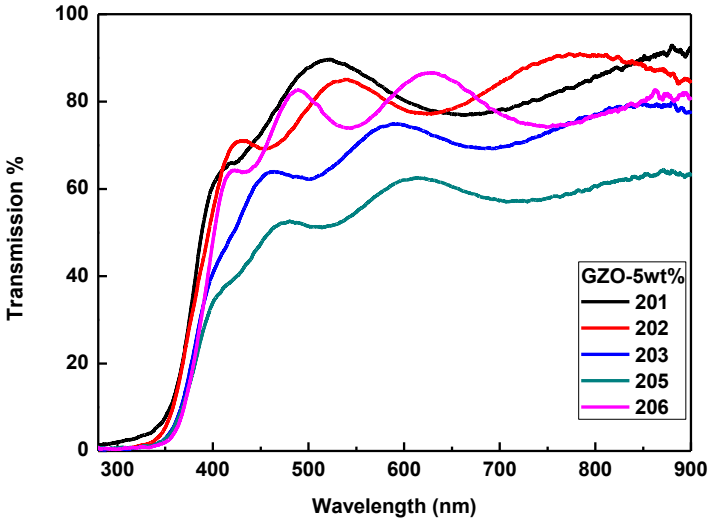

Figure 3.2-7 Transmission Spectra of GZO-5wt% Thin Films group

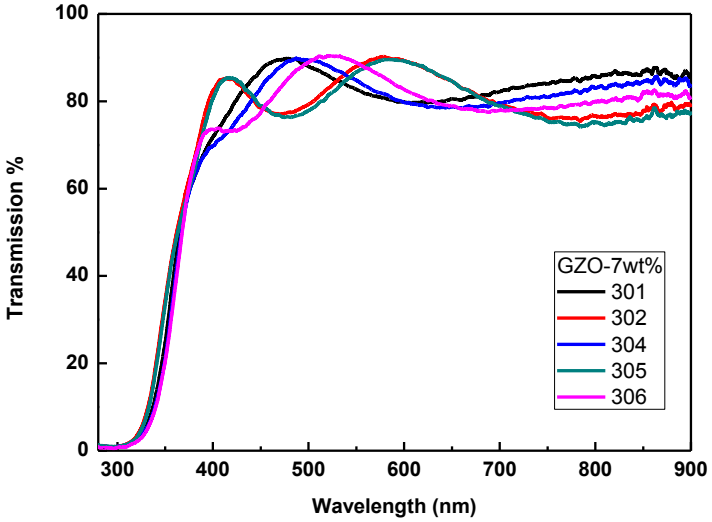

Figure 3.2-8 Transmission Spectra of GZO-7wt% thin films group

Considering Temperature as one of the deposition parameters in this study, a chosen recipe out of each group was tested with substrate heating at 200^{o}C. In case of GZO-5wt% thin films group only one recipe was chosen while for GZO-7wt% thin films group, three recipes were tested. GZO-5wt% -Sample-GZO-205 was deposited in the following conditions [100 sccm. 150 watt/ 10 mtorr] at room temperature, and sample-GZO-206 the same condition at 200^{o}C. While GZO-7wt% samples tested with substrates heating are GZO-304 and GZO-305 while GZO-306 was the same as GZO-304 except it was tested at 50 sccm (Ar) flow instead of 100 sccm (Ar) flow, all are shown in table [3.2 and 3.3].

The first thing noticed about adding substrate heating to the equation, is that the rate of deposition has increased significantly in GZO-5wt% group, where the rate of deposition jumped from 3 nm/min to 3.8 nm/min , while for GZO-7wt% the change in the rate wasn't much as it only increased by 1 nm/min to change from 2.1 nm/min to 2.2 nm/min for GZO-301 and GZO-304 respectively, and the change for GZO-302 and GZO-305 was 2.2 nm/min as the deposition rate changed from 2.4 nm/min to 2.6 nm/min.

XRD pattern for the two samples of GZO-5wt% are shown in Fig. [3.2.9], it didn't show significant change, No shift in the diffraction angle was observed, however it's noticed that the intensity of all three diffraction peaks that corresponds to (100), (002) and (101) planes are slightly decreased compared to the thin film deposited at (RT). Moreover, another plane started slightly to appear (102) in the sample where substrate heating was applied. The grain size only decreased by 2 nm to change from 11 nm for the thin film deposited at (RT) to 9 nm for the thin film deposited at 200 ^{o}C. No sign of any metallic phase of (Ga) was observed proving that the (Ga) has successfully substituted the (Zn) atoms in the lattice[54].

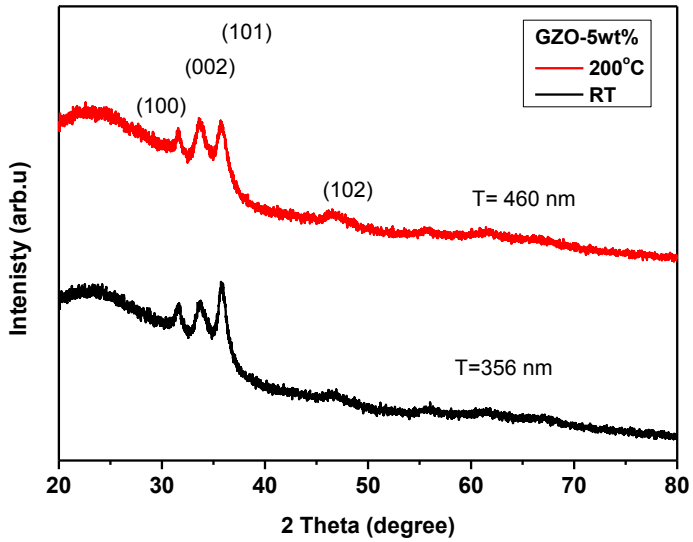

Figure 3.2-9 XRD patterns for GZO-wt5% as-deposited and Substrate heating

As mentioned earlier in this chapter, that GZO-7wt% thin film group shows only a dominant diffraction peak corresponding to (002) plane. The change over the XRD pattern for the GZO-7wt% thin films group due to substrate heating was observable. First, it's clear that the intensity of the peak decreased as the substrate heating was applied, shown in fig. [4.2.10] the XRD pattern for the thin films deposited in RT versus that deposited at 200^{o} C. it's quite different from annealing effect on the thin films where the preferred diffraction peaks intensity increase with annealing time and annealing temperature[1,15,16–18]. However, according to Z.Z. You and G.J. Huo et al. as the growth temperature increases, the intensity of (002) peak decreases[10]. Second observation was the slight appearance of a shoulder that corresponds to a diffraction peak of (101) plane on all GZO-7wt% thin films deposited at 200^{o} C, this can't be considered as much of change, however it indicates that increasing the growth temperature might result in the appearance of other phases that corresponds to the polycrystalline nature of the thin films. The third finding was the slight shift toward lower diffraction angles when comparing the (RT) samples and the growth temperature of 200^{o} C, as follow; RT-grown GZO-301 peak was shown at (2θ) of 34.1°, while the 200^{o} C-grown GZO-304 peak was shifted to the

left at 33.8°. The case was the same for GZO-302 and GZO-305 where the peaks were shown at 33.7° and 33.6° respectively. GZO-306 thin film sample was deposited under the same conditions of GZO-30 with one exception, 50 sccm of (Ar) flow instead of 100 sccm. As shown in Fig. [3.2.10] the observed change was the decrease in the intensity of the (002) peak and the slight shift towards the right side to higher diffraction angle, where the sample deposited at 100 sccm (Ar) flow showed peak at 33.85° and the sample deposited at 50 sccm (Ar) showed its peak at 34°, this shift to the higher diffraction angle is suggested to be due to the decrease in the inter-planer spacing[38].

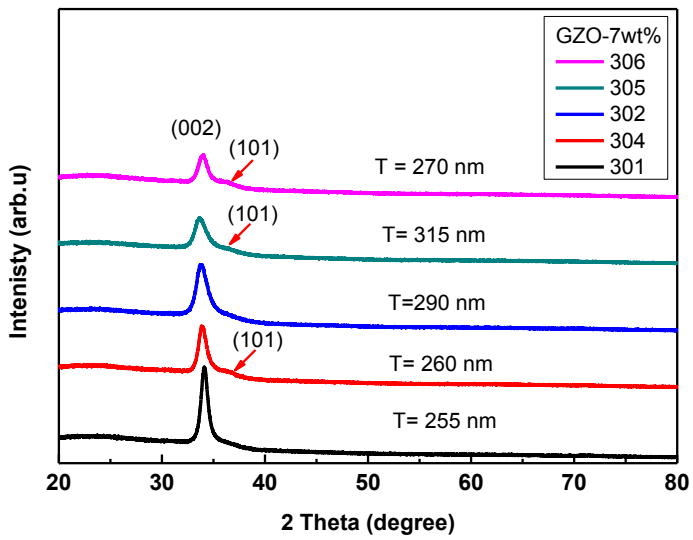

Figure 3.2-10 XRD Patterns of GZO-7wt%, at RT and 200 °C deposition

The effect of the growth temperature on the optical characteristics was observed on both groups of GZO. Fig. [3.2.11] shows the transmission spectra for both GZO-5wt% samples grown in (RT) and 200°C; it appears that applying temperature has improved the transmission significantly, as it jumped from 60% to above 75%. The (E_g) was reduced upon applying temperature to fall from [3.75 eV to 3.38 eV]. The effect of growth temperature however, had less effect on the GZO-7wt% thin film group when compared to the GZO-5wt% thin film group. As shown previously in

fig. [4.8] and Table [2.2 and 2.3] the transmission of the (200°C) grown films didn't change much from that of the thin films grown in (RT), where all thin films transmission kept above 82%. Moreover the change in (E_g) as shown in table [3.1], was not more than 0.5 eV.

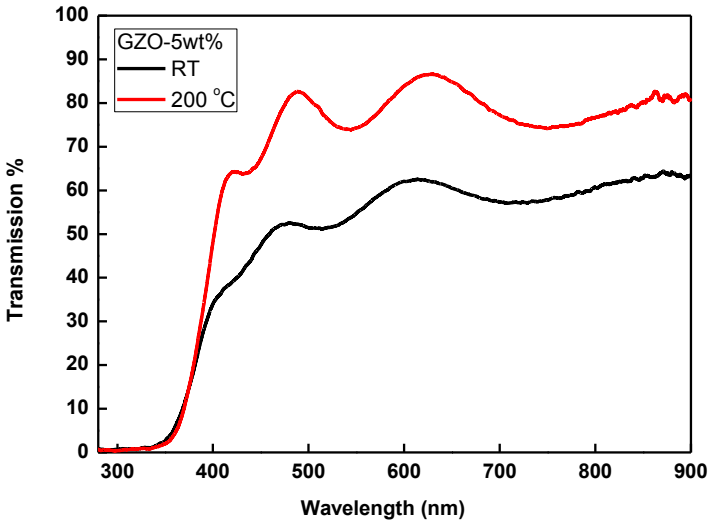

Figure 3.2-11 Transmission Spectra of GZo-5wt% grown at (RT) and 200 °C

In a nutshell, based on the Structural and optical data analysis, GZO-7wt% thin films group have shown more stable and reliable results compared to the GZO-5wt% thin films group. As the change in the deposition parameters didn't have much effect on the GZO-7wt% group as it did have on the GZO-5wt% group, where both transmission and (E_g) have significantly changed along with the grain size in the later.

After finalizing the XRD data interpretation and determining the optical properties, the rest of the characterization was performed on the GZO thin films deposited at RT and 200 C.

3.2.2. Chemical Composition and Electrical Properties

X-Ray Photoelectron Spectroscopy was performed for the two samples; GZO-205 and GZO-206 for GZO-5wt% thin film group, and GZO-301 and GZO-304 for the GZO-7wt%. These four samples are chosen to represent the (RT) grown thin films and the 200°C grown thin films.

XPS data for all of the four samples of GZO have shown the presence of the following peaks; C 1s, O 1s, Zn 2p and Ga 3d. The carbon peak was an indication for a major contamination that might be as a result of being exposed to the ambient atmosphere just as it appeared on the IZO thin films. As mentioned earlier the classification of O 1s peak positions , for both groups of the GZO-5wt% and GZO-7wt% thin films, O 1s peak lied in the low (BE) region which is an indication that the O^{-2} ions are embedded in the lattice [48] surrounded by Zn and Ga in GZO thin films.

For GZO thin films groups the O 1s peak observed at 532.1 eV, however there was a slight shift to the lower binding energy by 1 eV, was observed for the films deposited at 200 °C, showing the peak at 531.05 eV representing the O^{-2} in the oxygen deficient regions, this shift to the lower binding energy with increasing temperature is an indication for the reduction of oxygen vacancies. Moreover, Zn $2p_{3/2}$ and Zn $2p_{1/2}$ peaks of GZO groups were observed to be centered at 1021.9 and 1044.06 eV respectively, indicating that the Zn atoms remained in the valance state of Zn^{+2} within the GZO matrix, clearly the Zn metallic peak wasn't observed, which is in agreement with the XRD data, indicating that the Zn only exist in the oxidized state[10].

Ga 3d peak is centered at 18.34 eV corresponding to (Ga-O) bond proving the existence of the Ga in form of oxidized state. The atomic content of the deposited thin films determined by XPS were over looked by most of the literature, where all the focus were over the weight % (wt %) or the atomic % (at %) of the materials of the used targets not the deposited films. Taking into consideration the atomic percentage of the film contents revealed by the XPS data analysis, it was found that

the Ga atomic content was 4 at% and 7 at% for the GZO-5wt% and GZO-7wt% thin film groups respectively, while Zn atomic for both thin film groups content were recorded to be over 40 at%. The highest content was recorded for the Oxygen; it was over 45 % proving the oxide state of both Ga and Zn.

Using ezHEMS Hall Effect Measurement System, the electrical properties were determined for the deposited two thin films samples. Using van der pauw, a varied set of current was applied to the thin films ranging from 100 nA to 500 mA, to determine the electrical characteristics of the GZO thin films. Table [3.2.3] shows the electrical properties for the GZO thin films deposited at RT and at 200 °C. Apparently thin films grown at 200°C have shown an increase the mobility (μ) for all deposited thin films of both groups of GZO, although that the carrier concentration (η_e) kept their order of magnitude for each of the GZO thin films group. Taking thickness into consideration GZO-7% is around 260 nm while GZO-5% is around 460, the (η_e) as shown are higher in order of the one magnitude for the GZO-5%. Both of GZO groups have shown an increase in mobility (μ) with substrate heating giving [4.26, 4.98 $cm^2.V^{-1}.S^{-1}$] for GZO-5% and [3.08, 8.36 $cm^2.V^{-1}.S^{-1}$] for GZO-7%. As shown in table [3.2.2], the highest mobility was detected in GZO-7wt% thin film group in the film grown at 200 °C. Maybe As there was a slight decrease in the grain size as mentioned earlier, this decrease might have contributed in the mobility (μ) increment [59].

Table 3.2-2 Optical Bandgap (Eg) and electrical characteristics (ρ, ne, and μ) of GZO-5wt% and GZO-7wt% thin films

	GZO-205	**GZO-206**	**GZO-301**	**GZO-304**
Thickness (nm)	355	460	255	260
Resistivity (ρ) (Ω.cm)	0.0245	0.0589	0.2329	0.149
Carrier Density (η_e) (cm^{-3})	5.9×10^{19}	2.12×10^{19}	8.68×10^{18}	4.98×10^{18}
Mobility (μ) ($cm^{-2}.V^{-1}.S^{-1}$)	4.26	4.98	3.08	8.36
Optical Bandgap (E_g) (eV)	3.75	3.38	3.65	3.6

3.2.3. Morphological Structure

The morphology of GZO thin films are shown in Fig [3.2.12] that represents the 2D AFM images of these thin films. It's known that the deposition via sputtering is one of the PVD techniques that provide uniform deposition. However, a degree of roughness is always present in the thin films. Such roughness is a result of many factors; doping, deposition parameters and thin films thicknesses.

According to Jana S, et al. The thin films were expected to show different root mean square (RMS) roughness as a function of the gallium doping, where the higher roughness was recorded for the lower Ga doping[60]. In this study the GZO-5wt% present showed higher roughness than GZO-7wt%, however its worth mentioning that the thicknesses are playing a major role as well, where the thicknesses of the GZO-5wt% are nearly double the thicknesses of the GZO-7wt%.

In The GZO-5wt%, the thin film grown at RT with thickness are 356 nm, has shown RMS of 2.97 nm. That has increased a bit with the thin film grown at 200 C, as it has shown RMS of 4.43 nm that increase in the RMS is also a result of the higher thickness of 460 nm. The same behavior was observed for GZO-7wt%, where the roughness increased with the higher temperature. The RMS increased from 2.35 nm to 3.65 nm for the thin films grown as RT and 200 C, respectively.

Regarding the grain sizes, the AFM grain statistics has shown that the grain sizes of GZO-5wt% were 12 nm and 9 nm for the RT-grown thin film and that grown at 200 °C respectively, which is in agreement with the XRD calculations. While for GZO-7wt% the grain sizes were recorded to be 11 nm and 10 nm for the thin film grown at RT and the thin film grown at 200 °C respectively. Thicker films of 900 nm for both of the GZO were deposited for the sake of mechanical characterization. Their RMS was higher as expected recoding 4.27 nm for GZO-5wt% and 4.81 nm for GZO-7wt%.

a) b)

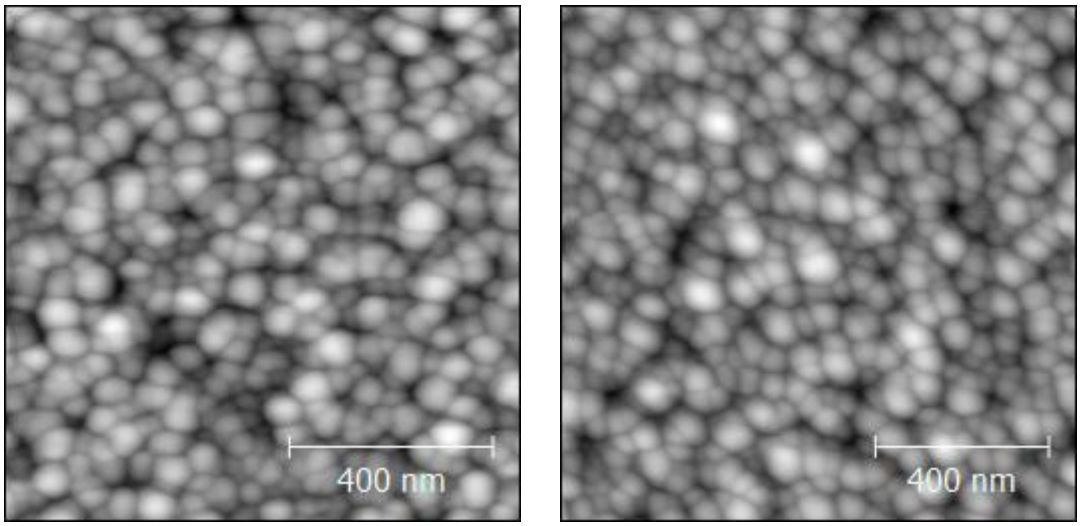

Figure 3.2-12 2D AFM images of GZO-7wt% GZO-5wt%, a) RT-grown, b) 200 °C

3.3. Indium Gallium Zinc Oxide Thin films (IGZO)

After discussing and exploring the characteristics of zinc oxide thin films doped with (In) and (Ga) separately in the previous sections, here in this section the characteristics of zinc oxide thin films doped with both (In/Ga) are being discussed. The samples here are also under investigation of the effect of deposition parameters on their characteristics. Table [3.4] shows the thin films deposition parameters for IGZO thin films group. First, as the previous material samples, the effect of RF-power, (Ar) flow as well as the substrate heating on the Crystallinity and optical characteristics are presented, then a comparison between RT-grown thin films and 200^{o}C- grown thin films is expressed further in terms of chemical composition, bond state, electrical, morphological and mechanical properties. The deposition time was fixed as well at 2 hours to determine the effect of deposition parameters on the rate of deposition.

3.3.1. Crystallinity and Optical properties

Starting with XRD, it's known that the IGZO thin films exhibit amorphous structure and it doesn't indicate any crystalline features unless heat treatment is applied above 600^{o}C[61–65,18]. In this study the amorphous nature of the IGZO didn't change with changing the deposition parameters neither at RT nor 200^{o}C. First, the pressure and (Ar) flow were fixed at 10 mtorr and 100 sccm respectively, while the RF-power was tested at 150watt and 100 watt to deposit samples IGZO-201 and IGZO-202 respectively. While Sample IGZO-204 was deposited under the same parameters as IGZO-202 except for the (Ar) flow where it was changes to 50 sccm instead of 100 sccm. The amorphous nature dominates as expected, No diffraction peaks was observed at any condition indicating the independency of the amorphous nature of the IGZO deposited thin films of any change in the deposition condition. However, the intensity of the amorphous feature appeared to decrease along with decreasing the RF-power to 100 watt, and to increase while decreasing (Ar) flow to 50 sccm.

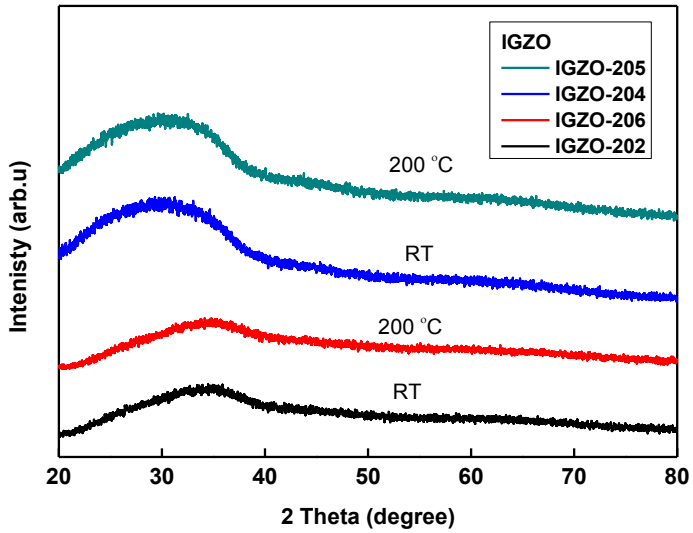

Figure 3.3-1 XRD Patters of IGZO Thin Films at RT and 200°C

Two more samples; IGZO-205 and IGZO-206 were deposited under the same conditions of IGZO-204 and IGZO-202 respectively, except that these films were grown at 200 °C. Fig [3.3.1] shows the XRD pattern of these for samples to compare between the wto sets of RT-grown thin films and 200°C-grown samples. As shown the amorphous feature still the dominant phase of the IGZO thin films grown at higher temperature, which agrees with X.F. Chen et al. and S. J. Seo et al. where their studies shown that the IGZO keeps its amorphous structure up to 600°C[48,18].

The Ellipsometery data were fitted as mentioned earlier, after which the film thicknesses were determined along with the optical constants. The rate of deposition only changed in order of 0.1nm/min, higher as the (Ar) flow decreased to 50 sccm instead of 100 sccm, where the thicknesses recorded to be 305 nm and 314 nm respectively. While the rate of deposition in case of increased growth temperature has a decrement in order of 0.1nm/min. Rate of depositions along with the films thicknesses are stated in table [3.4] In case of decreasing the RF power from 150 watt to 100 watt, the rate of deposition decreased by a value of 0.5nm/min. It's recognizable that the changing in deposition conditions doesn't have much effect on

the rate of deposition of IGZO group compared to the GZO-5wt% thin film groups, while it's similar to that of GZO-7wt%. As the optical constants were determined (n, k) the (E_g) were determined as well by ploting $(\alpha h\nu)^2$ versus ($h\nu$) and extrapolating the linear behavior which shows that the IGZO as well as all doped zinc oxide thin films in this study are of direct transition kind of semiconductors[66].

In this group of material, as mentioned earlier two recipes were grown at 200 °C compared to the RT-grown thin films, the following part will focus on that comparison, including [IGZO-202 & IGZO-206] as one set and [IGZO-204 & IGZO-205] as another.

Staring with the optical constants; in Fig [3.3.2 and 3.3.3] the plots of refractive indices (n) and extinction coefficients (k) are shown respectively. The change over the both (n) and (k) indicates the change over the bandgap as in fig[3.3.4] the plot of $(\alpha h\nu)^2$ versus ($h\nu$) is shown, from which the (E_g) is estimated. Table [3.3.1] represents the (E_g) of IGZO thin films group along with their transmittance. The changes over the (E_g) were very indicative, that the substrate heating caused the (E_g) to increase by 0.2 eV for both sets of IGZO. An explanation was presented by G. He et al. where he stated that the increase in growth temperature lead to an increment in the mobility of the atoms through the provided thermal energy, which in turn increase the atoms diffusion into the films resulting in less defect and more closely packed thin films. This causes the increase in Refractive index and in turn the (E_g) [48,67].

Moreover, it's known that the heat treatment enhances the surface morphology leading to better transmission[48,68]. However, IGZO is known of its high transmittance in the visible region, where in this study the substrate heating didn't have much effect on the transmission, except for the first sample that showed low transmission as 54%, all the others IGZO thin films showed transmission >80%. As shown in fig [3.3.5] the transmission of the two sets of IGZO as a function of substrate heating. In case of low (Ar) flow as 50 sccm, the effect of the 200°C was 2% difference, as it was recorded 84% at RT and 86% at 200°C. while the case was not the same at higher (Ar) flow of 100 sccm, where the temperature didn't affect

the transmission, keeping it almost the same except that a noticeable shift in the blue region towards higher energy, indicating the change over the (E_g), which comes in agreement with the results estimate from the fitted ellipsometery data.

Table 3.3-1 IGZO Thin Films Optical Bandgap

	E_g (eV)	**Transmission**		**E_g (eV)**	**Transmission**
IGZO-204	3.8	84%	**IGZO-202**	3.84	79%
IGZO-205	3.82	86%	**IGZO-206**	3.86	80%

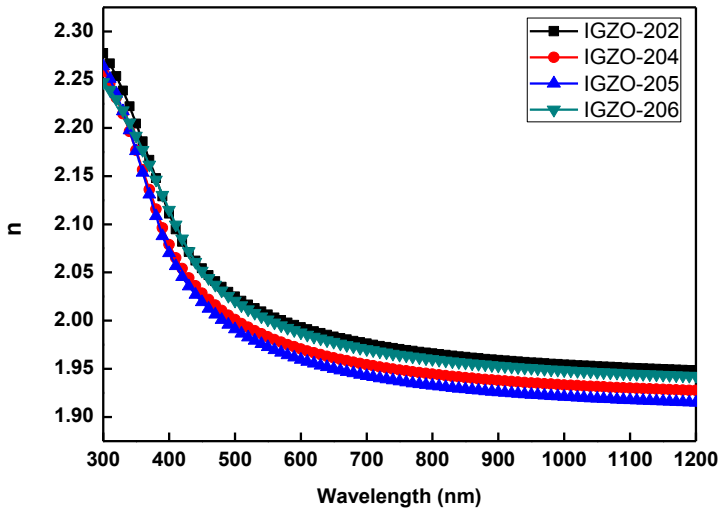

Figure 3.3-2 Refcractive Indices of IGZO thin films

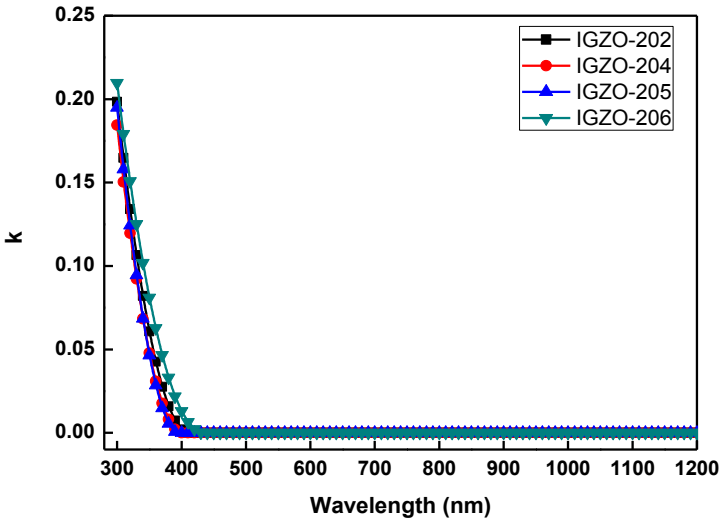

Figure 3.3-3 Extinction Coefficients (k) of IGZO Thin Films

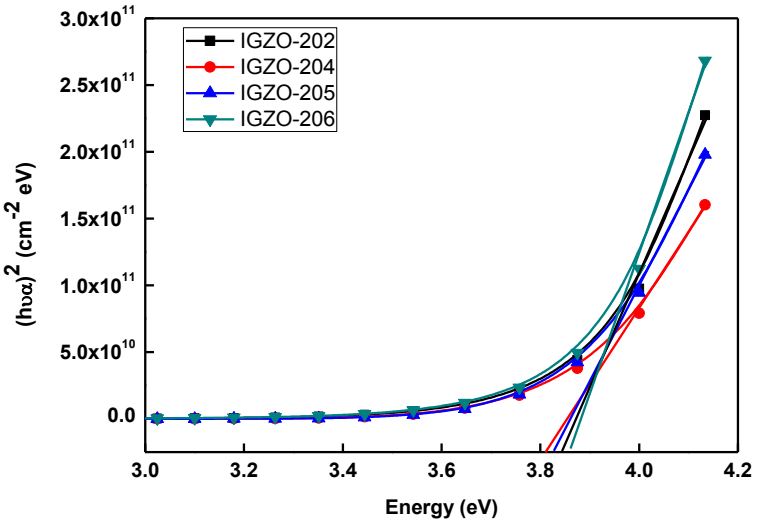

Figure 3.3-4 Plot of $(\alpha hv)^2$ versus (hv) for IGZO thin films

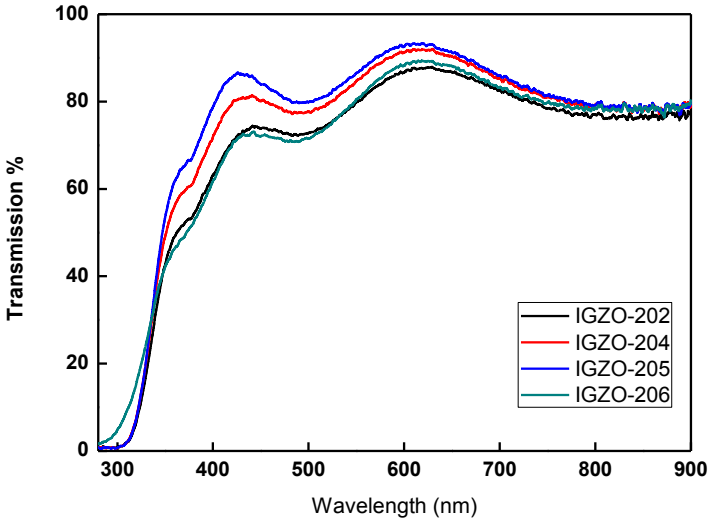

Figure 3.3-5 Transmission Spectra of IGZO thin films

3.3.2. Chemical Composition, Bond State and Electrical properties

Regarding the XPS data analysis, the same as IZO and GZO thin films groups, the samples deposited at RT and at 200 °C were investigated. Since this group of thin films belongs to the same kind of materials, it was expected to observe the same materials peaks that were observed in both IZO and GZO thin films groups. The full spectra showed the following peaks; C 1s, O 1s, Zn 2p and Ga 3d as well. The carbon peak was an indication for a major contamination that might be as a result of being exposed to the ambient atmosphere. For IGZO the Oxygen peak was centered at the lower binding energy centered at 530.7, which is characteristic to the loosely bound oxygen in the films, surprisingly with increasing temperature the shift was towards slightly higher binding energy to be 531 eV. The peaks for Ga $2p_{3/2}$ and Ga $2p_{1/2}$ were centered at 1117.7 & 1144.7 eV respectively corresponding to the (Ga-Zn) bond. There was a slight shift to the higher bonding energy with increasing

temperature to be 1118 eV for Ga $2p_{3/2}$ and 1145.12 eV for Ga $2p_{1/2}$. The case was the same for In 3d peak there was a slight shift to the higher binding energy with increasing temperature where the peaks of In $3d_{5/2}$ and In $3d_{3/2}$ shifted from 444.57 and 452.16 eV to 444.83 and 452.39 eV respectively indicating that the oxidation state of both (Ga) and (In) has increased with increasing temperature. The same as in the other materials groups, no metal peaks were observed for neither of (In) or (Ga) indicated that they are all existed in the oxide states

The electrical properties were determined by ezHEMS Hall System as well. The resistivity (ρ) along with carrier concentration (ηe) and mobility (μ) of these two thin films are shown in Table [3.3.2]. As can be indicated from the table, the thin film grown at 200 °C has shown higher carrier density. IGZO showed the same behavior for both of the IGZO thin films, where the measurements of (ρ) were recorded almost the same for both of the IGZO thin films [4.2 X 10^{-3} Ω.cm] for the RT-grown thin film and [4.4 X 10^{-3} Ω.cm] for the thin film grown at 200 °C. The (η_e) was measured as [3.2 x 10^{20} cm^{-3} and 3.6 x 10^{20} cm^{-3}] for thin film grown at RT and at 200 °C, respectively. Moreover, the mobility (μ) didn't change as well, recording values of 4.53 and 4.56 $cm^{-2}.V^{-1}.S^{-1}$] This indicates that the heat effect on the thin films is not significant, exactly the same as the heat effect on the other characteristics of the IGZO thin films. That might be because the IGZO thin film kept its amorphous features even under 200 °C, which agrees with literature, where the amorphous nature of the IGZO thin films starts to change at higher temperature over 600 °C.

Table 3.3-2 IGZO Thin Films Electrical Properties

Property	IGZO-204	IGZO-205
Thickness (nm)	314	310
Resistivity (ρ) (Ω.cm)	0.0042	0.0044
Carrier Density (η_e) (cm^{-3})	3.2×10^{20}	3.6×10^{20}
Mobility (μ) ($cm^{-2}. V^{-1}.S^{-1}$)	4.53	4.56

3.3.3. Morphological Structure

The morphology of the deposited IGZO thin film grown at RT and grown at 200 °C are shown in 2D AFM images in Fig. [3.3.6 & 3.3.7] The change in temperature didn't have much effect on the thin film where the roughness kept its value around 1 nm in both cases of thin films that might be an indication that the IGZO thin film preserved its amorphous nature without noticeable change over lower temperature as was shown by C.-H. Wu et al. that the IGZO thin films that they had grown at 200 C and 400 C have not change morphology wise not until 600 C[69], keeping in mind that the two thin films in this study also share similar thicknesses 314 and 310 nm. Moreover, these thin films show that they are uniform and smooth, which is one of the requirements in the TCE technology. This comes in agreement with our results from XRD and XPS as mentioned in sections 4.3.1 and 4.3.2. Moreover, this also comes in agreement with the literature where the amorphous nature of IGZO changes under the influence of higher temperatures over 600 °C[55,62–65,69,70,70]. The thicker film showed higher roughness around 2.5 nm. This come as a result of the discontinuous deposition of the IGZO as it was deposited a 3 time intervals each of 2 hours.

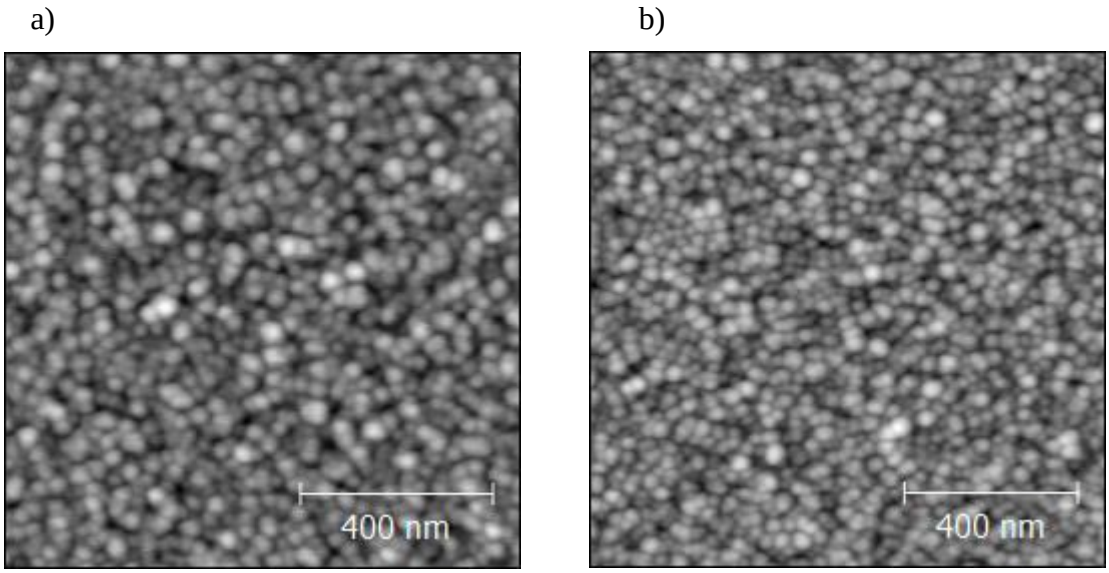

Figure 3.3-6 2D AFM image of IGZO grown at a) RT, b) 200 °C

3.4.Mechanical Characteristics of the Doped Zinc Oxide Thin Films; IZO, GZO and IGZO

Finally, for the mechanical characteristics, as mentioned earlier, thicker films were deposited around 900 nm only for both of GZO and IGZO. They were deposited on both silicon and glass substrates. Their thicknesses were 912 nm, 910 nm and 930 nm for GZO-5wt%, GZO-7wt% and IGZO respectively. While IZO thin film mechanical characterization was performed on the already deposited thin film. AFM-Nano-indentation was used to determine the Hardness (H) and Young's Modulus (E), which are shown in Table [3.4.1]. The values are quite lower than expected for the doped zinc oxide thin films. In the literature it's recorded in the range of [5-10 GPa] for (H) and [100-150 GPa] for (E) [71], however polycrystalline ZnO has resulted in (H) of a range of 1 GPa and (E) in range of 40 GPa [72]. This work results agree with the XRD results in this work indicating the polycrystalline feature of the deposited films, where the (H) of GZO-5% and GZO-7% were recorded as 3 GPa and 1.3 GPa respectively, while (E) recoreded to be 68 GPa and 47 GPa for GZO-5% and GZO-7% respectively on glass substrate. However, on silicon substrate (H) and (E) recorded even lower values, while it should have for the glass substrate because of its amorphous characteristics. This might be resulted upon the discontinuous growth of the thicker films where they were deposited on separate time intervals.

The same was seen by the IGZO film where it recoded (H) of 4 GPa and 0.3 GPa and (E) 94 GPa and 12 GPa each on glass and Si substrates respectively. These finding were also lower than expected[36,73,74]. The overall results were that on both silicon and glass substrates the (H) and (E) values were lower than recorded in the literature. This might be for two reasons, first the discontinuous deposition of these films that prevented the thin films to acquire the coherence, making these films many layers over each other instead of on coherent layer. Second reason is the possibility of considerable amount of contamination.

Table 3.4-1 Electrical Properties of the doped-ZnO thin films

Sample	**Thickness (nm)**	**Grain size (nm)**	**Hardness (GPa) Si**	**Elastic modulus (E) - Si**	**Hardness (GPa) glass**	**Elastic modulus (E) glass**
IZO	340	16	1.47	49	1.53	51
GZO-5wt%	912	12	1.5	50	3	68
GZO-7wt%	910	13	1.5	61	1.3	47
IGZO	930	----	0.3	12	4	94

Chapter 4

Conclusion and Future Prospective

4. Conclusion and future prospective

In summary this work reports the deposition of doped-ZnO on Si and glass substrate via RF sputtering magnetron and the dependence of structural, optical and electrical properties of IZO, GZO and IGZO on the deposition parameters, along with a comparative study between the doped-ZnO thin films grown at RT and at 200 °C substrate heating. It was found that as the temperature increases the grain size is slightly decreased in GZO groups resulting in increasing the films mobility as a result of enhancing the crystallinity which was also observed via the blue shift in the transmission spectra. The highest (μ) was recorded as 9.54 $cm^2.V^{-1}.S^{-1}$ and 8.3 $cm^2 V^{-1}.S^{-1}$ for IZO thin film grown at RT and GZO-7wt% thin film grown at 200 °C, respectively. IGZO mobility didn't change as the films kept their amorphous features with relatively low substrate heating temperature at 200 °C. The transmittance was fairly the same regardless of the substrate temperature in the visible region. Moreover, the films showed planes (100), (002) and (101) as

preferred orientation for GZO-5% while only (002) for GZO-7%. (H) and (E) have shown lower value than expected however, its due to many factors including the discontinuous deposition to acquire thicker films that causes the films to be incoherent in addition to the poly-crystallinity characteristics of the deposited films and due to the high thickness as well.

Table 4. 3 Effect of Deposition Parameters Increment on the Doped-ZnO Thin Films Characteristics

Effect of Increment	**IZO**	**GZO-5wt%**	**GZO-7wt**	**IGZO**
RF-Power				
Growth Rate	Increased	Increased	Slightly Increased	Increased
Transmission	Decreased	Increased	Increased	Increased
Grain size	Decreased	Decreased	Decreased	----------
(Ar) flow				
Growth Rate	Increased	Increased	Didn't change	Increased
Transmission	Decreased	Decreased	Decreased	Decreased
Grain size	Decreased	Slightly Increased	Slightly Increased	----------
Pressure				
Growth Rate	Decreased	Decreased	----------	----------
Transmission	Slightly Decreased	Decreased	----------	----------
Grain size	Decreased	Decreased	----------	----------

In general the output of these doped-ZnO thin films characteristics have shown three important results; first, that IZO in particular has shown promising characteristics at room temperature deposition that are quite applicable for TCO applications. Second, that the results of the low substrate heating have shown comparable results to the high temperature post-annealing process in literature. Showing that possibility of reducing the number of processes required to achieve enhanced characteristics,

resulting in saving time and cost. Third the results in general are represented as a primitive puzzle map that shows each parameters effect on the each characteristics that might help in determining the required deposition parameters for the specific desired characteristics and/or lead others to further studies of the deposition parameters effect for specific application. These results are shown as a summary in table [4.1] and table [4.2], as they are representing the effect of each deposition parameter on the characteristics of the doped-ZnO thin films.

Table 4. 4. Effect of Substrate Heating on the Doped-ZnO Thin Films Characteristics

Effect of 200 °C	**IZO**	**GZO-5wt%**	**GZO-7wt%**	**IGZO**
Rate of growth	Increased	Highly Increased	Slightly Increased	Slightly Increased
Transmission	Slightly Decreased	Increased	Increased	Increased
Optical Bandgap (Eg)	Slightly Increased	Decreased	Slightly Decreased	Increased by 0.02eV
Grain size	Slightly Increased	Slightly Decreased	No change	----------
Crystallinity	Enhanced	No change	No change	Amorphous
Surface roughness	Decreased	Increased	Increased	No Change
Resistivity	Slightly Decreased	Increased	Decreased	No Change
Carrier conc.	Slightly Increased	Decreased	Decreased	No Change
Mobility	Decreased	Slightly Increased	Increased	No Change

Suggested recommendation; is that further studies are definitely required to study the effect of the both deposition parameters and the substrate temperature on the mechanical properties of the doped-ZnO thin films. It would be more efficient to perform this study on the different substrates including silicon, glass, quarts as well as flexible polymers, which is essential for the flexible TCO and flexible electronic applications.

Bibliography

[1] Z.R. Dai, Z.W. Pan, Z.L. Wang, Novel nanostructures of functional oxides synthesized by thermal evaporation, Adv. Funct. Mater. 13 (2003) 9–24. doi:10.1002/adfm.200390013.

[2] L. Castaneda., Present Status of the Development and Application of Transparent Conductors Oxide Thin Solid Films, Mater. Sci. Appl. 2 (2011) 1233–1242. doi:10.4236/msa.2011.29167.

[3] D.J. Rogers, F. Hosseini Tehrani, ZnO : From Transparent Conducting Oxide to Transparent Electronics, Encycl. Mater. Sci. Technol. (2010) 1–5.

[4] Z.L. Wang, Nanobelts, nanowires, and nanodiskettes of semiconducting oxides - From materials to nanodevices, Adv. Mater. 15 (2003) 432–436. doi:10.1002/adma.200390100.

[5] Y. Ding, Z.L. Wang, Structures of planar defects in ZnO nanobelts and nanowires, Micron. 40 (2009) 335–342. doi:10.1016/j.micron.2008.10.008.

[6] Z.L. Wang, Z.W. Pan, Z.R. Dai, Structures of oxide nanobelts and nanowires, Microsc. Microanal. 8 (2002) 467–474. doi:10.1017/S1431927602010383.

[7] Thin Film Materials and Devices, in: Mater. Technol., n.d. doi:10.1016/B978-0-8155-1483-1.50002-2.

[8] K. Ellmer, A. Klein, B. Rech, Transparent Conductive Zin Oxide Basic and Applications in Thin Film Solar Cells, 2008. doi:10.1007/978-3-540-73612-7.

[9] E. Çetinörgü, S. Goldsmith, R.L. Boxman, The effect of annealing on filtered vacuum arc deposited ZnO thin films, Surf. Coatings Technol. 201 (2007) 7266–7272. doi:10.1016/j.surfcoat.2007.01.036.

[10] Z.Z. You, G.J. Hua, Electrical, optical and microstructural properties of transparent conducting GZO thin films deposited by magnetron sputtering, J. Alloys Compd. 530 (2012) 11–17. doi:10.1016/j.jallcom.2012.03.078.

[11] a. S. Pugalenthi, R. Balasundaraprabhu, V. Gunasekaran, N. Muthukumarasamy, S. Prasanna, S. Jayakumar, Effect of thickness on the structural, optical and electrical properties of RF magnetron sputtered GZO thin films, Mater. Sci. Semicond. Process. 29 (2015) 176–182. doi:10.1016/j.mssp.2014.02.014.

[12] A.G. Rolo, J. Ayres de Campos, T. Viseu, T. de Lacerda-Arôso, M.F. Cerqueira, The annealing effect on structural and optical properties of ZnO thin films produced by r.f. sputtering, Superlattices Microstruct. 42 (2007) 265–269. doi:10.1016/j.spmi.2007.04.069.

[13] D.-H. Kim, H. Jeon, G. Kim, S. Hwangboe, V.P. Verma, W. Choi, et al., Comparison of the optical properties of undoped and Ga-doped ZnO thin films deposited using RF magnetron sputtering at room temperature, Opt. Commun. 281 (2008) 2120–2125. doi:10.1016/j.optcom.2007.12.015.

[14] N.E. Duygulu, Effect of r.f. power variation on gallium doped zinc oxide thin films, Vacuum. 120 (2015) 19–27. doi:10.1016/j.vacuum.2015.05.036.

[15] M.V. Castro, C.J. Tavares, Dependence of Ga-doped ZnO thin film properties on different sputtering process parameters: Substrate temperature, sputtering pressure and bias voltage, Thin Solid Films. 586 (2015) 13–21. doi:10.1016/j.tsf.2015.04.036.

[16] H. Mahdhi, Z. Ben Ayadi, S. Alaya, J.L. Gauffier, K. Djessas, The effects of dopant concentration and deposition temperature on the structural, optical and electrical properties of Ga-doped ZnO thin films, Superlattices Microstruct. 72 (2014) 60–71. doi:10.1016/j.spmi.2014.04.013.

[17] J.H. Kim, B. Du Ahn, C.H. Kim, K.A. Jeon, H.S. Kang, S.Y. Lee, Heat generation properties of Ga doped ZnO thin films prepared by rf-magnetron sputtering for transparent heaters, Thin Solid Films. 516 (2008) 1330–1333. doi:10.1016/j.tsf.2007.03.100.

[18] S.J. Seo, J.H. Cho, Size control of nanocrystals in InGaZnO4 thin films fabricated by using the sol-gel method, J. Korean Phys. Soc. 60 (2012) 267. doi:10.3938/jkps.60.267.

[19] H. Wang, Y. Sun, L. Fang, L. Wang, B. Chang, X. Sun, et al., Growth and characterization of high transmittance GZO films prepared by sol-gel method, Thin Solid Films. 615 (2016) 19–24. doi:10.1016/j.tsf.2016.06.048.

[20] K. Tang, S. Gu, J. Liu, J. Ye, S. Zhu, Y. Zheng, Effects of indium doping on the crystallographic, morphological, electrical, and optical properties of highly crystalline ZnO films, J. Alloys Compd. 653 (2015) 643–648. doi:10.1016/j.jallcom.2015.09.051.

[21] J.-H. Kim, S.-M. Koo, Effect of epitaxial growth on electrical properties of Ga-doped ZnO thin films, Ceram. Int. 41 (2015) 37–42. doi:10.1016/j.ceramint.2014.07.053.

[22] J.A. Sans, J.F. Sánchez-Royo, A. Segura, Study of the bandgap renormalization in Ga-doped ZnO films by means of optical absorption under high pressure and photoelectron spectroscopy, Superlattices Microstruct. 43 (2008) 362–367. doi:10.1016/j.spmi.2007.12.020.

[23] Z.Z. Ye, J.F. Tang, Transparent conducting indium doped ZnO films by dc reactive S-gun magnetron sputtering., Appl. Opt. 28 (1989) 2817–9. doi:10.1364/AO.28.002817.

[24] D.G. Constantin, M. Apreutesei, R. Arvinte, A. Marin, O.C. Andrei, D. Munteanu, Magnetron sputtering technique used for coatings deposition; technologies and applications, 7th Int. Conf. Mater. Sci. Eng. – BRAMAT 2011. (2011) 24–26.

[25] W. Kern, K.K. Schuegraf, Deposition Technologies and Applications: Introduction and Overview, Handb. Thin-Film Depos. Process. Tech. i (2002).

[26] C. a Moore, Z. Yu, L.R. Thompson, G.J. Collins, 9 - Laser and Electron Beam Assisted Processing, (2001) 349–379. doi:http://dx.doi.org/10.1016/B978-081551442-8.50014-6.

[27] W.S. Knodle, R. Chow, 10 - Molecular Beam Epitaxy: Equipment and Practice, Handb. Thin Film Depos. Process. Tech. (Second Ed. (2001) 381–461. doi:http://dx.doi.org/10.1016/B978-081551442-8.50015-8.

[28] S. Rossnagel, Sputtering and Sputter Deposition., Handb. Thin-Film Depos. Process. Technol. (2001) 319–348. doi:10.1002/ange.19891010662.

[29] J.L. Zilko, Metal Organic Chemical Vapor Deposition : Technology and Equipment, Thin-Film Depos. Process. Technol. (2001) 151–203. doi:10.1016/B978-081551442-8.50009-2.

[30] M.L. Hammond, Silicon Epitaxy by Chemical Vapor Deposition, Handb. Thin Film Depos. Process. Thechniques Princ. Methods, Equip. Appl. (2001) 45–126. doi:http://dx.doi.org/10.1016/B978-081551442-8.50007-9.

[31] C.E. Kim, P. Moon, I. Yun, S. Kim, J.M. Myoung, H.W. Jang, et al., Process estimation and optimized recipes of ZnO:Ga thin film characteristics for transparent electrode applications, Expert Syst. Appl. 38 (2011) 2823–2827. doi:10.1016/j.eswa.2010.08.074.

[32] C.H. Huang, D.Y. Chen, C.Y. Hsu, Influence of deposition parameters and annealing treatment on the properties of GZO films grown using rf magnetron sputtering, Ceram. Int. 38 (2012) 1057–1063. doi:10.1016/j.ceramint.2011.08.031.

[33] T. Film, G. Process, 2 Thin Film Processes, in: n.d. doi:10.1016/B978-0-8155-1483-1.50003-4.

[34] D. Depla, S. Mahieu, J. Greene, Sputter deposition processes, Handb. Depos. Technol. Film. Coatings. 281 (1991) 253–296. http://books.google.com/books?hl=en&lr=&id=owMVeiPmQaAC&oi=fnd&pg=PA177&dq=Sputter+deposition+processes&ots=L4r5OnYaVv&sig=yN2iwxGU5Y11BArgoAH14zMydUw.

[35] S. Yield, 3 Sputtering Phenomena, in: Energy, 1852. doi:10.1016/B978-0-8155-1483-1.50004-6.

[36] E. Seker, S. Pat, Nanomechanical and elastic properties of TiN coated dental materials determined by atomic force microscopy, 9 (2015) 460–463.

[37] S.K. Wang, T.C. Lin, S.R. Jian, J.Y. Juang, J.S.C. Jang, J.Y. Tseng, Effects of post-annealing on the structural and nanomechanical properties of Ga-doped ZnO thin films deposited on glass substrate by rf-magnetron sputtering, Appl. Surf. Sci. 258 (2011) 1261–1266. doi:10.1016/j.apsusc.2011.09.088.

[38] S. Chen, M.E.A. Warwick, R. Binions, Effects of film thickness and thermal treatment on the structural and opto-electronic properties of Ga-doped ZnO films deposited by sol–gel method, Sol. Energy Mater. Sol. Cells. 137 (2015) 202–209. doi:10.1016/j.solmat.2015.02.016.

[39] N. Ito, Y. Sato, P.K. Song, A. Kaijio, K. Inoue, Y. Shigesato, Electrical and optical properties of amorphous indium zinc oxide films, Thin Solid Films. 496 (2006) 99–103. doi:10.1016/j.tsf.2005.08.257.

[40] D.Y. Ku, I.H. Kim, I. Lee, K.S. Lee, T.S. Lee, J. h. Jeong, et al., Structural and electrical properties of sputtered indium-zinc oxide thin films, Thin Solid Films. 515 (2006) 1364–1369. doi:10.1016/j.tsf.2006.03.040.

[41] W. Lim, Y.-L. Wang, F. Ren, D.P. Norton, I.I. Kravchenko, J.M. Zavada, et al., Indium zinc oxide thin films deposited by sputtering at room temperature, Appl. Surf. Sci. 254 (2008) 2878–2881. doi:10.1016/j.apsusc.2007.10.032.

[42] S.C. Chang, M.H. Shiao, Smooth indium zinc oxide film prepared by sputtering a In2O3:ZnO=95:5 target, Microelectronics J. 38 (2007) 1202–1206. doi:10.1016/j.mejo.2007.09.014.

[43] C. Lee, W. Lee, H. Kim, H.W. Kim, Influence of annealing atmosphere on the structure, resistivity and transmittance of InZnO thin films, Ceram. Int. 34 (2008) 1089–1092. doi:10.1016/j.ceramint.2007.09.053.

[44] J.-W. Jeon, D.-W. Jeon, T. Sahoo, M. Kim, J.-H. Baek, J.L. Hoffman, et al., Effect of annealing temperature on optical band-gap of amorphous indium zinc oxide film, J. Alloys Compd. 509 (2011) 10062–10065. doi:10.1016/j.jallcom.2011.08.033.

[45] C. Li, J.H. Hsieh, S.J. Liu, W.S. Lin, Electrical and structural study on indium zinc oxide thin films by sputtering process, Surf. Coatings Technol. 231 (2013) 471–477. doi:10.1016/j.surfcoat.2012.04.084.

[46] A. Singh, S. Chaudhary, D.K. Pandya, Acta Materialia High conductivity indium doped ZnO fi lms by metal target reactive, Acta Mater. 111 (2016) 1–9. doi:10.1016/j.actamat.2016.03.012.

[47] Z.C. Jin, I. Hamberg, C.G. Granqvist, Optical properties of sputter-deposited

ZnO:Al thin films, J. Appl. Phys. 64 (1988) 5117–5131. doi:10.1063/1.342419.

[48] X.F. Chen, G. He, J. Gao, J.W. Zhang, D.Q. Xiao, P. Jin, et al., Substrate temperature dependent structural, optical and electrical properties of amorphous InGaZnO thin films, J. Alloys Compd. 632 (2015) 533–539. doi:10.1016/j.jallcom.2015.01.143.

[49] J. Chen, L. Wang, X. Su, L. Kong, G. Liu, X. Zhang, InGaZnO semiconductor thin film fabricated using pulsed laser deposition, 18 (2010) 38–41.

[50] N. Kumar, T.M. Wilkinson, C.E. Packard, M. Kumar, Design of low surface roughness-low residual stress-high optoelectronic merit a-IZO thin films for flexible OLEDs, J. Appl. Phys. 119 (2016) 225303. doi:10.1063/1.4953212.

[51] C.-Y. Chen, J.-J. Ho, Performance Evaluation of Indium Zinc Oxide Thin Films for Flexible Organic Light-emitting Device Applications, COIN-NGNCON 2006 - Jt. Int. Conf. Opt. Internet Next Gener. Netw. (2006) 262–264. doi:10.1109/COINNGNCON.2006.4454567.

[52] L.L. Ong, Z.Y.Z. Hong, C.Y.Y. Ang, J.H. Ou, Preparation , structure and optical properties of transparent conducting gallium-doped zinc oxide thin films, 33 (2015) 470–481. doi:10.1515/msp-2015-0065.

[53] Z.Z. You, G.J. Hua, Refractive index, optical bandgap and oscillator parameters of organic films deposited by vacuum evaporation technique, Vacuum. 83 (2009) 984–988. doi:10.1016/j.vacuum.2008.11.010.

[54] S.R. Jian, G.J. Chen, S.K. Wang, T.C. Lin, J.S.C. Jang, J.Y. Juang, et al., Rapid thermal annealing effects on the structural and nanomechanical properties of Ga-doped ZnO thin films, Surf. Coat. Technol. 231 (2013) 176–179. doi:10.1016/j.surfcoat.2012.06.060.

[55] H.S. Shin, B. Du Ahn, K.H. Kim, J.S. Park, H.J. Kim, The effect of thermal annealing sequence on amorphous InGaZnO thin film transistor with a plasma-treated source-drain structure, Thin Solid Films. 517 (2009) 6349–6352. doi:10.1016/j.tsf.2009.02.071.

[56] T. Yamada, A. Miyake, H. Makino, N. Yamamoto, T. Yamamoto, Effect of thermal annealing on electrical properties of transparent conductive Ga-doped ZnO films prepared by ion-plating using direct-current arc discharge, Thin Solid Films. 517 (2009) 3134–3137. doi:10.1016/j.tsf.2008.11.081.

[57] H. Makino, N. Yamamoto, A. Miyake, T. Yamada, Y. Hirashima, H. Iwaoka, et al., Influence of thermal annealing on electrical and optical properties of Ga-doped ZnO thin films, Thin Solid Films. 518 (2009) 1386–1389. doi:10.1016/j.tsf.2009.09.093.

[58] B. Du Ahn, S. Hoon Oh, C. Hee Lee, G. Hee Kim, H. Jae Kim, S. Yeol Lee,

Influence of thermal annealing ambient on Ga-doped ZnO thin films, J. Cryst. Growth. 309 (2007) 128–133. doi:10.1016/j.jcrysgro.2007.09.014.

[59] H.-K. Kim, K.-J. Ahn, H. Jang, H. Lee, Dependence of Electrical, Optical, and Structural Properties on the Thickness of GZO Films Prepared by CRMS, J. Electrochem. Soc. 159 (2012) H38. doi:10.1149/2.047201jes.

[60] M. Pal, S. Bera, H. Khan, S. Jana, Effect of Ga doping on Microstructural , Optical and Photocatalytic Properties of Nanostructured Zinc Oxide Thin Films, 50 (2015) 40–50.

[61] S.H. Chen, H.C. Liu, C.Y. Lee, J.Y. Gan, H.W. Zan, J.C. Hwang, et al., High performance electric-double-layer amorphous IGZO thin-film transistors gated with hydrated bovine serum albumin protein, Org. Electron. Physics, Mater. Appl. 24 (2015) 200–204. doi:10.1016/j.orgel.2015.05.046.

[62] L. Li, L. Fan, Y. Li, Z. Song, F. Ma, C. Liu, Effect of thermal annealing on the properties of transparent conductive In–Ga–Zn oxide thin films, J. Vac. Sci. Technol. A Vacuum, Surfaces, Film. 32 (2014) 21506. doi:10.1116/1.4861352.

[63] H. Bae, J.-H. Kwon, S. Chang, M.-H. Chung, T.-Y. Oh, J.-H. Park, et al., The effect of annealing on amorphous indium gallium zinc oxide thin film transistors, Thin Solid Films. 518 (2010) 6325–6329. doi:10.1016/j.tsf.2010.02.073.

[64] X. Li, E. Xin, L. Chen, J. Shi, C. Li, J. Zhang, Dependence of annealing on stability of transparent amorphous InGaZnO thin film transistor, Mater. Sci. Semicond. Process. 16 (2013) 1292–1296. doi:10.1016/j.mssp.2013.02.013.

[65] Q. Li, Z.X. Song, F. Ma, Y.H. Li, K.W. Xu, Effects of high-temperature thermal annealing on the electronic properties of In-Ga-Zn oxide thin films, J. Vac. Sci. Technol. A Vacuum, Surfaces, Film. 33 (2015) 21520. doi:10.1116/1.4908157.

[66] C.M. Hsu, W.C. Tzou, C.F. Yang, Y.J. Liou, Investigation of the high mobility IGZO thin films by using co-sputtering method, Materials (Basel). 8 (2015) 2769–2781. doi:10.3390/ma8052769.

[67] G. He, L.Q. Zhu, M. Liu, Q. Fang, L.D. Zhang, Optical and electrical properties of plasma-oxidation derived HfO2 gate dielectric films, Appl. Surf. Sci. 253 (2007) 3413–3418. doi:10.1016/j.apsusc.2006.07.055.

[68] D. Han, S. Zhang, F. Zhao, J. Dong, Y. Cong, S. Zhang, et al., Transparent gallium doped zinc oxide thin- fi lm transistors fabricated on glass substrate, Thin Solid Films. 594 (2015) 266–269. doi:10.1016/j.tsf.2015.06.026.

[69] C.H. Wu, G.J. Jiang, K.W. Chang, C.W. Lin, K.L. Chen, Highly sensitive amorphous In-Ga-Zn-O films for ppb-level ozone sensing: Effects of deposition temperature, Sensors Actuators, B Chem. 211 (2015) 354–358.

doi:10.1016/j.snb.2015.01.048.

[70] D.P. Pham, H.T. Nguyen, B.T. Phan, V.D. Hoang, S. Maenosono, C.V. Tran, Influence of addition of indium and of post-annealing on structural, electrical and optical properties of gallium-doped zinc oxide thin films deposited by direct-current magnetron sputtering, Thin Solid Films. 583 (2015) 201–204. doi:10.1016/j.tsf.2015.03.068.

[71] E. Materials, ZnO Deposited, (2005) 169–173.

[72] Ü.Ö. Hadis Morkoç, Zinc Oxide: Fundamentals, Materials and Device Technology, 2009. doi:10.1002/9783527623945.ch1.

[73] D.W. Mohammed, R. Waddingham, A.J. Flewitt, K.A. Sierros, J. Bowen, S.N. Kukureka, Mechanical properties of amorphous indium-gallium-zinc oxide thin films on compliant substrates for flexible optoelectronic devices, Thin Solid Films. 594 (2015) 197–204. doi:10.1016/j.tsf.2015.09.052.

[74] W.C. Oliver, G.M. Pharr, Measurement of hardness and elastic modulus by instrumented indentation: Advances in understanding and refinements to methodology, J. Mater. Res. 19 (2004) 3–20. doi:10.1557/jmr.2004.19.1.3.